Measurement of the top pair production cross section in the dilepton decay channel in $p\bar{p}$ collisions at $\sqrt{s} = 1.96$ TeV

T. Aaltonen,[22] B. Álvarez González,[10,x] S. Amerio,[42a] D. Amidei,[33] A. Anastassov,[37] A. Annovi,[18] J. Antos,[13] G. Apollinari,[16] J. A. Appel,[16] A. Apresyan,[47] T. Arisawa,[56] A. Artikov,[14] J. Asaadi,[52] W. Ashmanskas,[16] B. Auerbach,[59] A. Aurisano,[52] F. Azfar,[41] W. Badgett,[16] A. Barbaro-Galtieri,[27] V. E. Barnes,[47] B. A. Barnett,[24] P. Barria,[45a,45c] P. Bartos,[13] M. Bauce,[42a,42b] G. Bauer,[31] F. Bedeschi,[45a] D. Beecher,[29] S. Behari,[24] G. Bellettini,[45a,45b] J. Bellinger,[58] D. Benjamin,[15] A. Beretvas,[16] A. Bhatti,[49] M. Binkley,[16,a] D. Bisello,[42a,42b] I. Bizjak,[29,dd] K. R. Bland,[5] C. Blocker,[7] B. Blumenfeld,[24] A. Bocci,[15] A. Bodek,[48] D. Bortoletto,[47] J. Boudreau,[46] A. Boveia,[12] B. Brau,[16,c] L. Brigliadori,[6a,6b] A. Brisuda,[13] C. Bromberg,[34] E. Brucken,[22] M. Bucciantonio,[45a,45b] J. Budagov,[14] H. S. Budd,[48] S. Budd,[23] K. Burkett,[16] G. Busetto,[42a,42b] P. Bussey,[20] A. Buzatu,[32] S. Cabrera,[15,z] C. Calancha,[30] S. Camarda,[4] M. Campanelli,[34] M. Campbell,[33] F. Canelli,[12,16] A. Canepa,[44] B. Carls,[23] D. Carlsmith,[58] R. Carosi,[45a] S. Carrillo,[17,m] S. Carron,[16] B. Casal,[10] M. Casarsa,[16] A. Castro,[6a,6b] P. Catastini,[16] D. Cauz,[53a] V. Cavaliere,[45a,45c] M. Cavalli-Sforza,[4] A. Cerri,[27,h] L. Cerrito,[29,s] Y. C. Chen,[1] M. Chertok,[8] G. Chiarelli,[45a] G. Chlachidze,[16] F. Chlebana,[16] K. Cho,[26] D. Chokheli,[14] J. P. Chou,[21] W. H. Chung,[58] Y. S. Chung,[48] C. I. Ciobanu,[43] M. A. Ciocci,[45a,45c] A. Clark,[19] D. Clark,[7] G. Compostella,[42a,42b] M. E. Convery,[16] J. Conway,[8] M. Corbo,[43] M. Cordelli,[18] C. A. Cox,[8] D. J. Cox,[8] F. Crescioli,[45a,45b] C. Cuenca Almenar,[59] J. Cuevas,[10,x] R. Culbertson,[16] D. Dagenhart,[16] N. d'Ascenzo,[43,v] M. Datta,[16] P. de Barbaro,[48] S. De Cecco,[50a] G. De Lorenzo,[4] M. Dell'Orso,[45a,45b] C. Deluca,[4] L. Demortier,[49] J. Deng,[15,e] M. Deninno,[6a] F. Devoto,[22] M. d'Errico,[42a,42b] A. Di Canto,[45a,45b] B. Di Ruzza,[45a] J. R. Dittmann,[5] M. D'Onofrio,[28] S. Donati,[45a,45b] P. Dong,[16] T. Dorigo,[42a] K. Ebina,[56] A. Elagin,[52] A. Eppig,[33] R. Erbacher,[8] D. Errede,[23] S. Errede,[23] N. Ershaidat,[43,cc] R. Eusebi,[52] H. C. Fang,[27] S. Farrington,[41] M. Feindt,[25] J. P. Fernandez,[30] C. Ferrazza,[45a,45d] R. Field,[17] G. Flanagan,[47,t] R. Forrest,[8] M. J. Frank,[5] M. Franklin,[21] J. C. Freeman,[16] I. Furic,[17] M. Gallinaro,[49] J. Galyardt,[11] J. E. Garcia,[19] A. F. Garfinkel,[47] P. Garosi,[45a,45c] H. Gerberich,[23] E. Gerchtein,[16] S. Giagu,[50a,50b] V. Giakoumopoulou,[3] P. Giannetti,[45a] K. Gibson,[46] C. M. Ginsburg,[16] N. Giokaris,[3] P. Giromini,[18] M. Giunta,[45a] G. Giurgiu,[24] V. Glagolev,[14] D. Glenzinski,[16] M. Gold,[36] D. Goldin,[52] N. Goldschmidt,[17] A. Golossanov,[16] G. Gomez,[10] G. Gomez-Ceballos,[31] M. Goncharov,[31] O. González,[30] I. Gorelov,[36] A. T. Goshaw,[15] K. Goulianos,[49] A. Gresele,[42a] S. Grinstein,[4] C. Grosso-Pilcher,[12] R. C. Group,[16] J. Guimaraes da Costa,[21] Z. Gunay-Unalan,[34] C. Haber,[27] S. R. Hahn,[16] E. Halkiadakis,[51] A. Hamaguchi,[40] J. Y. Han,[48] F. Happacher,[18] K. Hara,[54] D. Hare,[51] M. Hare,[55] R. F. Harr,[57] K. Hatakeyama,[5] C. Hays,[41] M. Heck,[25] J. Heinrich,[44] M. Herndon,[58] S. Hewamanage,[5] D. Hidas,[51] A. Hocker,[16] W. Hopkins,[16,i] D. Horn,[25] S. Hou,[1] R. E. Hughes,[38] M. Hurwitz,[12] U. Husemann,[59] N. Hussain,[32] M. Hussein,[34] J. Huston,[34] G. Introzzi,[45a] M. Iori,[50a,50b] A. Ivanov,[8,q] E. James,[16] D. Jang,[11] B. Jayatilaka,[15] E. J. Jeon,[26] M. K. Jha,[6a] S. Jindariani,[16] W. Johnson,[8] M. Jones,[47] K. K. Joo,[26] S. Y. Jun,[11] T. R. Junk,[16] T. Kamon,[52] P. E. Karchin,[57] Y. Kato,[40,p] W. Ketchum,[12] J. Keung,[44] V. Khotilovich,[52] B. Kilminster,[16] D. H. Kim,[26] H. S. Kim,[26] H. W. Kim,[26] J. E. Kim,[26] M. J. Kim,[18] S. B. Kim,[26] S. H. Kim,[54] Y. K. Kim,[12] N. Kimura,[56] S. Klimenko,[17] K. Kondo,[56] D. J. Kong,[26] J. Konigsberg,[17] A. Korytov,[17] A. V. Kotwal,[15] M. Kreps,[25] J. Kroll,[44] D. Krop,[12] N. Krumnack,[5,n] M. Kruse,[15] V. Krutelyov,[52,f] T. Kuhr,[25] M. Kurata,[54] S. Kwang,[12] A. T. Laasanen,[47] S. Lami,[45a] S. Lammel,[16] M. Lancaster,[29] R. L. Lander,[8] K. Lannon,[38,w] A. Lath,[51] G. Latino,[45a,45c] I. Lazzizzera,[42a] T. LeCompte,[2] E. Lee,[52] H. S. Lee,[12] J. S. Lee,[26] S. W. Lee,[52,y] S. Leo,[45a,45b] S. Leone,[45a] J. D. Lewis,[16] C.-J. Lin,[27] J. Linacre,[41] M. Lindgren,[16] E. Lipeles,[44] A. Lister,[19] D. O. Litvintsev,[16] C. Liu,[46] Q. Liu,[47] T. Liu,[16] S. Lockwitz,[59] N. S. Lockyer,[44] A. Loginov,[59] D. Lucchesi,[42a,42b] J. Lueck,[25] P. Lujan,[27] P. Lukens,[16] G. Lungu,[49] J. Lys,[27] R. Lysak,[13] R. Madrak,[16] K. Maeshima,[16] K. Makhoul,[31] P. Maksimovic,[24] S. Malik,[49] G. Manca,[28,d] A. Manousakis-Katsikakis,[3] F. Margaroli,[47] C. Marino,[25] M. Martínez,[4] R. Martínez-Ballarín,[30] P. Mastrandrea,[50a] M. Mathis,[24] M. E. Mattson,[57] P. Mazzanti,[6a] K. S. McFarland,[48] P. McIntyre,[52] R. McNulty,[28,k] A. Mehta,[28] P. Mehtala,[22] A. Menzione,[45a] C. Mesropian,[49] T. Miao,[16] D. Mietlicki,[33] A. Mitra,[1] G. Mitselmakher,[17] H. Miyake,[54] S. Moed,[21] N. Moggi,[6a] M. N. Mondragon,[16,m] C. S. Moon,[26] R. Moore,[16] M. J. Morello,[16] J. Morlock,[25] P. Movilla Fernandez,[16] A. Mukherjee,[16] Th. Muller,[25] P. Murat,[16] M. Mussini,[6a,6b] J. Nachtman,[16,o] Y. Nagai,[54] J. Naganoma,[56] I. Nakano,[39] A. Napier,[55] J. Nett,[58] C. Neu,[44,bb] M. S. Neubauer,[23] J. Nielsen,[27,g] L. Nodulman,[2] O. Norniella,[23] E. Nurse,[29] L. Oakes,[41] S. H. Oh,[15] Y. D. Oh,[26] I. Oksuzian,[17] T. Okusawa,[40] R. Orava,[22] L. Ortolan,[4] S. Pagan Griso,[42a,42b] C. Pagliarone,[53a] E. Palencia,[10,h] V. Papadimitriou,[16] A. A. Paramonov,[2] J. Patrick,[16] G. Pauletta,[53a,53b] M. Paulini,[11] C. Paus,[31] D. E. Pellett,[8] A. Penzo,[53a] T. J. Phillips,[15] G. Piacentino,[45a] E. Pianori,[44] J. Pilot,[38] K. Pitts,[23] C. Plager,[9] L. Pondrom,[58] K. Potamianos,[47] O. Poukhov,[14,a] F. Prokoshin,[14,aa] A. Pronko,[16] F. Ptohos,[18,j] E. Pueschel,[11] G. Punzi,[45a,45b] J. Pursley,[58] A. Rahaman,[46] V. Ramakrishnan,[58] N. Ranjan,[47] I. Redondo,[30] P. Renton,[41] M. Rescigno,[50a] F. Rimondi,[6a,6b] L. Ristori,[45a,16] A. Robson,[20] T. Rodrigo,[10] T. Rodriguez,[44]

E. Rogers,[23] S. Rolli,[55] R. Roser,[16] M. Rossi,[53a] F. Ruffini,[45a,45c] A. Ruiz,[10] J. Russ,[11] V. Rusu,[16] A. Safonov,[52] W. K. Sakumoto,[48] L. Santi,[53a,53b] L. Sartori,[45a] K. Sato,[54] V. Saveliev,[43,v] A. Savoy-Navarro,[43] P. Schlabach,[16] A. Schmidt,[25] E. E. Schmidt,[16] M. P. Schmidt,[59,a] M. Schmitt,[37] T. Schwarz,[8] L. Scodellaro,[10] A. Scribano,[45a,45c] F. Scuri,[45a] A. Sedov,[47] S. Seidel,[36] Y. Seiya,[40] A. Semenov,[14] F. Sforza,[45a,45b] A. Sfyrla,[23] S. Z. Shalhout,[8] T. Shears,[28] P. F. Shepard,[46] M. Shimojima,[54,u] S. Shiraishi,[12] M. Shochet,[12] I. Shreyber,[35] A. Simonenko,[14] P. Sinervo,[32] A. Sissakian,[14,a] K. Sliwa,[55] J. R. Smith,[8] F. D. Snider,[16] A. Soha,[16] S. Somalwar,[51] V. Sorin,[4] P. Squillacioti,[16] M. Stanitzki,[59] R. St. Denis,[20] B. Stelzer,[32] O. Stelzer-Chilton,[32] D. Stentz,[37] J. Strologas,[36] G. L. Strycker,[33] Y. Sudo,[54] A. Sukhanov,[17] I. Suslov,[14] K. Takemasa,[54] Y. Takeuchi,[54] J. Tang,[12] M. Tecchio,[33] P. K. Teng,[1] J. Thom,[16,i] J. Thome,[11] G. A. Thompson,[23] E. Thomson,[44] P. Ttito-Guzmán,[30] S. Tkaczyk,[16] D. Toback,[52] S. Tokar,[13] K. Tollefson,[34] T. Tomura,[54] D. Tonelli,[16] S. Torre,[18] D. Torretta,[16] P. Totaro,[53a,53b] M. Trovato,[45a,45d] Y. Tu,[44] N. Turini,[45a,45c] F. Ukegawa,[54] S. Uozumi,[26] A. Varganov,[33] E. Vataga,[45a,45d] F. Vázquez,[17,m] G. Velev,[16] C. Vellidis,[3] M. Vidal,[30] I. Vila,[10] R. Vilar,[10] M. Vogel,[36] G. Volpi,[45a,45b] P. Wagner,[44] R. L. Wagner,[16] T. Wakisaka,[40] R. Wallny,[9] S. M. Wang,[1] A. Warburton,[32] D. Waters,[29] M. Weinberger,[52] W. C. Wester III,[16] B. Whitehouse,[55] D. Whiteson,[44,e] A. B. Wicklund,[2] E. Wicklund,[16] S. Wilbur,[12] F. Wick,[25] H. H. Williams,[44] J. S. Wilson,[38] P. Wilson,[16] B. L. Winer,[38] P. Wittich,[16,i] S. Wolbers,[16] H. Wolfe,[38] T. Wright,[33] X. Wu,[19] Z. Wu,[5] K. Yamamoto,[40] J. Yamaoka,[15] U. K. Yang,[12,r] Y. C. Yang,[26] W.-M. Yao,[27] G. P. Yeh,[16] K. Yi,[16,o] J. Yoh,[16] K. Yorita,[56] T. Yoshida,[40,l] G. B. Yu,[15] I. Yu,[26] S. S. Yu,[16] J. C. Yun,[16] A. Zanetti,[53a] Y. Zeng,[15] and S. Zucchelli[6a,6b]

(CDF Collaboration)[b]

[1]*Institute of Physics, Academia Sinica, Taipei, Taiwan 11529, Republic of China*
[2]*Argonne National Laboratory, Argonne, Illinois 60439, USA*
[3]*University of Athens, 157 71 Athens, Greece*
[4]*Institut de Fisica d'Altes Energies, Universitat Autonoma de Barcelona, E-08193, Bellaterra (Barcelona), Spain*
[5]*Baylor University, Waco, Texas 76798, USA*
[6a]*Istituto Nazionale di Fisica Nucleare Bologna, I-40127 Bologna, Italy;*
[6b]*University of Bologna, I-40127 Bologna, Italy*
[7]*Brandeis University, Waltham, Massachusetts 02254, USA*
[8]*University of California, Davis, Davis, California 95616, USA*
[9]*University of California, Los Angeles, Los Angeles, California 90024, USA*
[10]*Instituto de Fisica de Cantabria, CSIC-University of Cantabria, 39005 Santander, Spain*
[11]*Carnegie Mellon University, Pittsburgh, Pennsylvania 15213, USA*
[12]*Enrico Fermi Institute, University of Chicago, Chicago, Illinois 60637, USA*
[13]*Comenius University, 842 48 Bratislava, Slovakia; Institute of Experimental Physics, 040 01 Kosice, Slovakia*
[14]*Joint Institute for Nuclear Research, RU-141980 Dubna, Russia*
[15]*Duke University, Durham, North Carolina 27708, USA*
[16]*Fermi National Accelerator Laboratory, Batavia, Illinois 60510, USA*
[17]*University of Florida, Gainesville, Florida 32611, USA*
[18]*Laboratori Nazionali di Frascati, Istituto Nazionale di Fisica Nucleare, I-00044 Frascati, Italy*
[19]*University of Geneva, CH-1211 Geneva 4, Switzerland*
[20]*Glasgow University, Glasgow G12 8QQ, United Kingdom*
[21]*Harvard University, Cambridge, Massachusetts 02138, USA*
[22]*Division of High Energy Physics, Department of Physics, University of Helsinki and Helsinki Institute of Physics, FIN-00014, Helsinki, Finland*
[23]*University of Illinois, Urbana, Illinois 61801, USA*
[24]*The Johns Hopkins University, Baltimore, Maryland 21218, USA*
[25]*Institut für Experimentelle Kernphysik, Karlsruhe Institute of Technology, D-76131 Karlsruhe, Germany*
[26]*Center for High Energy Physics, Kyungpook National University, Daegu 702-701, Korea; Seoul National University, Seoul 151-742, Korea; Sungkyunkwan University, Suwon 440-746, Korea; Korea Institute of Science and Technology Information, Daejeon 305-806, Korea; Chonnam National University, Gwangju 500-757, Korea; Chonbuk National University, Jeonju 561-756, Korea*
[27]*Ernest Orlando Lawrence Berkeley National Laboratory, Berkeley, California 94720, USA*
[28]*University of Liverpool, Liverpool L69 7ZE, United Kingdom*
[29]*University College London, London WC1E 6BT, United Kingdom*
[30]*Centro de Investigaciones Energeticas Medioambientales y Tecnologicas, E-28040 Madrid, Spain*
[31]*Massachusetts Institute of Technology, Cambridge, Massachusetts 02139, USA*

[32]*Institute of Particle Physics, McGill University, Montréal, Québec, Canada H3A 2T8; Simon Fraser University, Burnaby, British Columbia, Canada V5A 1S6; University of Toronto, Toronto, Ontario, Canada M5S 1A7; and TRIUMF, Vancouver, British Columbia, Canada V6T 2A3*
[33]*University of Michigan, Ann Arbor, Michigan 48109, USA*
[34]*Michigan State University, East Lansing, Michigan 48824, USA*
[35]*Institution for Theoretical and Experimental Physics, ITEP, Moscow 117259, Russia*
[36]*University of New Mexico, Albuquerque, New Mexico 87131, USA*
[37]*Northwestern University, Evanston, Illinois 60208, USA*
[38]*The Ohio State University, Columbus, Ohio 43210, USA*
[39]*Okayama University, Okayama 700-8530, Japan*
[40]*Osaka City University, Osaka 588, Japan*
[41]*University of Oxford, Oxford OX1 3RH, United Kingdom*
[42a]*Istituto Nazionale di Fisica Nucleare, Sezione di Padova-Trento, I-35131 Padova, Italy;*
[42b]*University of Padova, I-35131 Padova, Italy*
[43]*LPNHE, Universite Pierre et Marie Curie/IN2P3-CNRS, UMR7585, Paris, F-75252 France*
[44]*University of Pennsylvania, Philadelphia, Pennsylvania 19104, USA*
[45a]*Istituto Nazionale di Fisica Nucleare Pisa, I-56127 Pisa, Italy;*
[45b]*University of Pisa, I-56127 Pisa, Italy;*
[45c]*University of Siena, I-56127 Pisa, Italy;*
[45d]*Scuola Normale Superiore, I-56127 Pisa, Italy*
[46]*University of Pittsburgh, Pittsburgh, Pennsylvania 15260, USA*
[47]*Purdue University, West Lafayette, Indiana 47907, USA*
[48]*University of Rochester, Rochester, New York 14627, USA*
[49]*The Rockefeller University, New York, New York 10065, USA*
[50a]*Istituto Nazionale di Fisica Nucleare, Sezione di Roma 1;*
[50b]*Sapienza Università di Roma, I-00185 Roma, Italy*
[51]*Rutgers University, Piscataway, New Jersey 08855, USA*
[52]*Texas A&M University, College Station, Texas 77843, USA*
[53a]*Istituto Nazionale di Fisica Nucleare Trieste/Udine, I-34100 Trieste, Italy;*

[a]Deceased
[b]With visitors from
[c]University of Massachusetts Amherst, Amherst, MA 01003, USA
[d]Istituto Nazionale di Fisica Nucleare, Sezione di Cagliari, 09042 Monserrato (Cagliari), Italy
[e]University of California Irvine, Irvine, CA 92697, USA
[f]University of California Santa Barbara, Santa Barbara, CA 93106, USA
[g]University of California Santa Cruz, Santa Cruz, CA 95064, USA
[h]CERN,CH-1211 Geneva, Switzerland
[i]Cornell University, Ithaca, NY 14853, USA
[j]University of Cyprus, Nicosia CY-1678, Cyprus
[k]University College Dublin, Dublin 4, Ireland
[l]University of Fukui, Fukui City, Fukui Prefecture, Japan 910-0017
[m]Universidad Iberoamericana, Mexico D.F., Mexico
[n]Iowa State University, Ames, IA 50011, USA
[o]University of Iowa, Iowa City, IA 52242, USA
[p]Kinki University, Higashi-Osaka City, Japan 577-8502
[q]Kansas State University, Manhattan, KS 66506, USA
[r]University of Manchester, Manchester M13 9PL, England
[s]Queen Mary, University of London, London, E1 4NS, England
[t]Muons, Inc., Batavia, IL 60510, USA
[u]Nagasaki Institute of Applied Science, Nagasaki, Japan
[v]National Research Nuclear University, Moscow, Russia
[w]University of Notre Dame, Notre Dame, IN 46556, USA
[x]Universidad de Oviedo, E-33007 Oviedo, Spain
[y]Texas Tech University, Lubbock, TX 79609, USA
[z]IFIC (CSIC-Universitat de Valencia), 56071 Valencia, Spain
[aa]Universidad Tecnica Federico Santa Maria, 110v Valparaiso, Chile
[bb]University of Virginia, Charlottesville, VA 22906, USA
[cc]Yarmouk University, Irbid 211-63, Jordan
[dd]On leave from J. Stefan Institute, Ljubljana, Slovenia

[53b]*University of Trieste/Udine, I-33100 Udine, Italy*
[54]*University of Tsukuba, Tsukuba, Ibaraki 305, Japan*
[55]*Tufts University, Medford, Massachusetts 02155, USA*
[56]*Waseda University, Tokyo 169, Japan*
[57]*Wayne State University, Detroit, Michigan 48201, USA*
[58]*University of Wisconsin, Madison, Wisconsin 53706, USA*
[59]*Yale University, New Haven, Connecticut 06520, USA*
(Received 16 February 2010; published 23 September 2010)

A measurement of the $t\bar{t}$ production cross section in $p\bar{p}$ collisions at $\sqrt{s} = 1.96$ TeV using events with two leptons, missing transverse energy, and jets is reported. The data were collected with the CDF II detector. The result in a data sample corresponding to an integrated luminosity 2.8 fb^{-1} is $\sigma_{t\bar{t}} = 6.27 \pm 0.73(\text{stat}) \pm 0.63(\text{syst}) \pm 0.39(\text{lum})$ pb. for an assumed top mass of 175 GeV$/c^2$.

DOI: 10.1103/PhysRevD.82.052002 PACS numbers: 14.65.Ha, 12.38.Qk, 13.85.Qk

I. INTRODUCTION

This paper describes a measurement of the $t\bar{t}$ production cross section in $p\bar{p}$ collisions at $\sqrt{s} = 1.96$ TeV with the CDF detector at the Fermilab Tevatron. This measurement requires the identification of both leptons in the decay chain $t\bar{t} \to (W^+b)(W^-\bar{b}) \to (\ell^+\nu_\ell b)(\ell^-\bar{\nu}_\ell\bar{b})$. Events are selected with two high transverse energy leptons: high missing transverse energy ($\not\!\!E_T$) and at least two jets in the final state. From the excess of events selected in the data over the predicted background from other known standard model (SM) sources, we obtain a measurement of the production of $t\bar{t}$ events.

The top quark pair production in the standard model proceeds primarily by quark-antiquark annihilations. At the Tevatron the predictions are 85% quark-antiquark annihilations and 15% gluon fusions. At the Large Hadron Collider at $\sqrt{s} = 14$ TeV the situation is predicted to be very different with 90% of the production being due to gluon-gluon fusion and 10% due to quark-antiquark annihilation.

This analysis improves upon a previous measurement of the cross section using the same dilepton (DIL) selection in a data sample with an integrated luminosity of 0.197 fb^{-1} [1]. Unlike other CDF measurements of the $t\bar{t}$ cross section in the dilepton channel [2], where one ℓ is identified as e or μ while the other is identified by the presence of a high momentum central track, the DIL analysis positively identifies both leptons as either electrons or muons from W decays or as products of semileptonic decays of τ leptons, thus allowing for the comparison of the observed yield of $t\bar{t}$ decays to ee, $\mu\mu$, and $e\mu$ final states with the predictions from lepton universality.

The measurement provides a test of the QCD calculations of the $t\bar{t}$ cross section [3] in a channel which is independent and complementary to other measurements of the $t\bar{t}$ cross section in higher statistics final states where at least one W boson from the top quark is reconstructed via its hadronic decay, $W \to qq'$. The dilepton final state suffers from a lower statistical precision, as the product of the branching ratios of the semileptonic W decay $\text{BR}(W^+ \to \ell^+\nu) \times \text{Br}(W^- \to \ell^-\nu) \approx 5\%$ with $\ell = e$ or μ, but it has a signal to background ratio well above unity even before requiring the identification of one of the jets originating from a b quark. This analysis does not require jets in the events to have secondary vertices consistent with the presence of a b-hadron decay as this selection would further reduce the acceptance by almost 50%.

In Sec. II we give a short description of the detector. In Sec. III the data sample and event selection are presented. Section IV presents the formula used for the cross section calculation and the measurement of the $t\bar{t}$ acceptance in dilepton events. Section V describes the calculation of the backgrounds. Systematics uncertainties are covered in Sec. VI. In Sec. VII observations are compared to predictions in control samples characterized by the presence of two leptons plus high $\not\!\!E_T$ in the final state. We conclude by presenting the result of our measurement in Sec. IX, followed by a short summary in Sec. X.

II. DETECTOR

CDF II is a general-purpose detector that is described in detail elsewhere [4]. The components relevant to this analysis are briefly described here. The detector has an approximate full angular coverage with a charged-particle tracker inside a magnetic solenoid, backed by calorimeters and muon detectors. CDF uses a cylindrical coordinate system in which θ is the polar angle about an axis defined by the proton beam and ϕ is the azimuthal angle about the beam axis. Particle pseudorapidity is defined as $\eta = -\ln\tan(\theta/2)$.

The charged-particle tracking system surrounds the beam pipe and consists of multiple layers of silicon micro-strip detectors, which cover a pseudorapidity region $|\eta| < 2$, and a 3.1 m long open-cell drift chamber covering the pseudorapidity region $|\eta| < 1$ [5,6]. The tracking system is located inside a superconducting solenoid, which in turn is surrounded by calorimeters. The magnetic field has a strength of 1.4 T and is aligned coaxially with the p and $\bar{p}$ beams.

The calorimeter system [7] is split radially into electromagnetic and hadronic sections segmented in projective tower geometry and covers the pseudorapidity range $|\eta| < 3.6$. The electromagnetic sampling calorimeters are constructed of alternating layers of lead absorber and scintillator whereas the hadronic calorimeters use iron absorbers. The central strip chambers are embedded in the central electromagnetic calorimeter at a depth of about $6X_0$ (radiation length), which is the region of maximum shower intensity for electrons. In the plug region stereo layers of scintillator bars are placed at shower maximum.

A set of central muon drift chambers located outside the central calorimeters (CMU), complemented by another set of central muon chambers set behind a 60 cm iron shield (CMP), provides muon coverage for $|\eta| \leq 0.6$. Additional drift chambers and scintillation counters (CMX) detect muons in the region $0.6 \leq |\eta| \leq 1.0$ [8].

Multicell gas Cerenkov counters [9] located in the $3.7 < |\eta| < 4.7$ region measure the average number of inelastic $p\bar{p}$ collisions per bunch crossing and thus determine the beam luminosity. The total uncertainty on the luminosity is estimated to be 5.9%, of which 4.4% comes from the acceptance and operation of the luminosity monitor and 4.0% from the uncertainty in the inelastic $p\bar{p}$ cross section.

III. DATA SAMPLE AND EVENT SELECTION

This analysis is based on an integrated luminosity of 2.8 fb^{-1} collected with the CDF II detector between March 2002 and April 2008. The data are collected with an inclusive lepton trigger that requires an electron (muon) with $E_T > 18$ GeV ($p_T > 18$ GeV/c). The transverse energy and transverse momentum are defined as $E_T = E\sin\theta$ and $p_T = p\sin\theta$, where E is energy measured in the calorimeter and p is momentum measured by the tracking system. From this inclusive lepton data set, events with a reconstructed isolated electron of E_T (muon of p_T) greater than 20 GeV(GeV/c) are selected. Isolation is defined as the calorimeter energy deposited in a cone of radius $\Delta R \equiv \sqrt{(\Delta\eta)^2 + (\Delta\phi)^2} = 0.4$ in $\eta - \phi$ space centered around the lepton, minus the energy deposited by the lepton itself. Details on electron and muon identification, or lepton ID, criteria used in this analysis are contained in Ref. [10]. Electrons are identified by matching clusters of localized energy deposition in the calorimeter to tracks reconstructed using hits from the tracking chambers and the extra constraint provided by the position of the beam line in the transverse direction. We further require that the energy deposition in the electromagnetic section of the calorimeter exceeds the energy measured in the corresponding hadronic section and the lateral cluster energy profile agrees with shapes derived from electron beam test data. Muons are identified by matching tracks to minimum ionizing-like clusters in the calorimeter and to stubs, or sets of radially aligned hits, in the muon chambers. Leptons passing all of the lepton identification cuts and also having isolation less than 10% of the lepton energy are defined as ''tight''. They can be of one of four categories: electrons reconstructed in the central electromagnetic (CEM) or plug electromagnetic (PHX from ''Phoenix'' the name of the tracking algorithm) calorimeter and muons pointing to the regions covered by both layers of CMU and CMP chambers (CMUP) or by the central muon extension chambers (CMX). These tight leptons are also required to be the objects that trigger the event, with the exception of PHX electrons which are allowed in events triggered by non-isolated CEM, CMUP, or CMX.

A second electron of E_T (muon of p_T) greater than 20 GeV(GeV/c) is also required using looser identification cuts and without the isolation requirement. ''Loose'' leptons are either electrons or muons which pass the same identification cuts as the tight leptons but fail the isolation requirement. Another category of loose leptons has no tight lepton counterpart and is made of muons with tracks pointing to regions covered by only one of the two central muon chambers (CMU, CMP) or with tracks of energy deposition corresponding to a minimum ionizing particle and pointing to regions not covered by a muon chamber (CMIO). CMIO muons, as well as PHX electrons, must be isolated.

Each dilepton candidate must contain at least one tight lepton and at most one loose lepton. These requirements result in 18 different DIL dilepton categories, as illustrated in Sec. IV A, where background estimates and acceptances are calculated separately for each category. Events with more than two tight or loose leptons in the final state are rejected as they come mostly from background sources like WZ and ZZ events. Another source of trilepton background comes from Drell-Yan $Z/\gamma^* \rightarrow e^+e^-$ events with a radiated photon converting into an asymmetric e^+e^- pair, that is a conversion pair where one electron does not reach the minimum track p_T threshold of 500 MeV/c needed for the electron to not be trapped inside the tracking chamber. The loss in signal efficiency from removal of events with three or more leptons is only 0.4%.

A fraction of events passing the dilepton selection does not originate from $p\bar{p}$ collisions but from beam interactions with the detector and shielding material or from cosmic ray sources. These events are removed by requiring a reconstructed vertex consistent with originating from the beam interaction region and within 60 cm of the center of the detector along the z direction. We also require that the timing of tracks in dimuon events be consistent with both muons traveling from the center of the detector outward into the tracking chamber [11]. Electrons from conversions of photons in the detector material are removed by identifying events with a track near the electron track of opposite curvature and consistent with coming from a $\gamma \rightarrow e^+e^-$ vertex.

Jets are reconstructed from the calorimeter towers using a cone algorithm with fixed radius $\Delta\text{R} = 0.4$ in $\eta - \phi$ space [12]. The jet E_T is corrected for detector effects due

to calorimeter dead zones and to nonlinear tower response to deposited energy. These effects are convoluted to provide the jet energy scale (JES) correction factor which estimates the energy of the originating parton from the measured energy of a jet [13]. Jets used in the DIL selection are required to have corrected $E_T > 15$ GeV and $|\eta| < 2.5$.

We further impose two cuts based on the kinematical properties of the event: the first is a cut on the missing transverse energy $\not\!\!E_T$ [1] which measures the transverse energy of the neutrinos via the imbalance of the energy detected in the calorimeter, after correcting for the presence of muons. We require that $\not\!\!E_T > 25$ GeV, which is strengthened to $a > 50$ GeV requirement if any lepton or jet is closer than 20° to the $\not\!\!E_T$ direction. This cut, in the following referred to as L-cut, is used to reject mainly $Z \rightarrow \tau^+\tau^-$ and events with mismeasured $\not\!\!E_T$ generated by jets pointing to cracks in the calorimeter. The second, or Z-veto cut, aims at reducing the contamination of dilepton decays of the Z boson by requiring high missing E_T significance for ee and $\mu\mu$ events with dilepton invariant mass in the 76–106 GeV/c^2 region. Missing E_T significance, or MetSig, is defined as $\not\!\!E_T/\sqrt{E_T^{\rm sum}}$, where $E_T^{\rm sum}$ is the sum of transverse energies deposited in all calorimeter towers. This variable separates events with real $\not\!\!E_T$ due to neutrinos from events where the $\not\!\!E_T$ is due to energy measurement fluctuations or energy loss in calorimeter cracks. This second category of events is expected to have a degraded $\not\!\!E_T$ resolution. In the DIL selection, we use a cut of MetSig > 4 GeV$^{(1/2)}$.

Events in the DIL dilepton sample passing the L-cut and Z-veto cut become $t\bar{t}$ candidate events if they have at least 2 jets, if the two leptons are of opposite charge, and if H_T the transverse energy sum of leptons, neutrinos, and jets is greater than 200 GeV. Events in the DIL dilepton sample reconstructed with 0 or 1 jet are used as control samples for the background estimation.

IV. CROSS SECTION

In this analysis we measure the cross section by using the formula

$$\sigma_{t\bar{t}} = \frac{\mathrm{N_{obs}} - \mathrm{N_{bkg}}}{\mathcal{A} \times \mathcal{L}}, \tag{1}$$

where $\mathrm{N_{obs}}$ is the number of dilepton candidate events, and $\mathrm{N_{bkg}}$ is the total background. The denominator is the product for the acceptance for $t\bar{t}$ candidate events, $\mathcal{A}$, and of the data set luminosity $\mathcal{L}$.

[1]The scalar quantity $\not\!\!E_T$ is the magnitude of the missing transverse energy vector $\not\!\!\vec{E}_T$ defined as the opposite of the sum over the calorimeter towers $\sum_i E_T^i \boldsymbol{n}_i$ of the transverse energy measured in each tower, E_T^i, times the unit vector in the azimuthal plane that points from the beam line to the ith calorimeter tower, $\boldsymbol{n}_i$.

The acceptance, which in our definition includes the effects of the detector geometrical acceptance, lepton identification, and $t\bar{t}$ to dilepton selection, is measured using the PYTHIA Monte Carlo program [14] to simulate $t\bar{t}$ events of all three decay modes (hadronic, lepton + jets, and dilepton) with an assumed $\mathrm{M_{top}} = 175$ GeV/c^2. Monte Carlo simulated events are required to have both W bosons from top quarks decaying to a lepton plus neutrino, where the lepton can be either an electron or muon. The $t\bar{t}$ Monte Carlo simulation acceptance prediction of 0.808 ± 0.004(stat)% is corrected by taking into account differences observed between data and the Monte Carlo simulation modeling of the detector response in independent control samples. The following sections describe the implementation and checks on the acceptance correction procedure.

A. Signal acceptance

The available statistics for each subsample of DIL events can be maximized by requiring that only detector parts essential for the identification of a particular lepton category be fully functioning. For example, PHX electrons require hits in the silicon inner vertex detector to reconstruct their tracks. Hence the identification of events with PHX electrons is limited to data taken with ''good,'' i.e. fully functioning, silicon detectors but no such requirements are imposed on events where the electron is central. To accommodate this approach, we rewrite the denominator of the cross section formula in Eq. (1) as the sum of the acceptance for each DIL category $\mathcal{A}_i$, weighted by the luminosity relative to that category $\mathcal{L}_i$:

$$\mathcal{A} \times \mathcal{L} = \sum_i \mathcal{A}_i \times \mathcal{L}_i. \tag{2}$$

In this analysis four different luminosity samples are used, corresponding to the integrated luminosity of runs with fully functional subdetectors for trigger CEM electrons and CMUP muons, either ignoring the status of the silicon detectors (2826 pb^{-1}) or requiring good silicon (2676 pb^{-1}), and runs fully functional also for trigger CMX muons, either ignoring (2760 pb^{-1}) or requiring (2623 pb^{-1}) good silicon. In defining runs good for CEM, CMUP, or CMX leptons, the distinction between isolated and nonisolated leptons is irrelevant.

The acceptances $\mathcal{A}_i$ can be factorized in terms of the two leptons ℓ_1 and ℓ_2 comprising the DIL category i according to the following formula:

$$\mathcal{A}_i = \mathcal{A}_{\ell_1\ell_2} \times \mathrm{C}_{\ell_1\ell_2}, \tag{3}$$

where the $\mathcal{A}_{\ell_1\ell_2}$ are the raw PYTHIA $t\bar{t}$ Monte Carolo (MC) efficiencies for events with reconstructed leptons ℓ_1 and ℓ_2 passing the full DIL selection and the $\mathrm{C}_{\ell_1\ell_2}$ are correction factors specific for that lepton pair. The correction factors are in turn calculated as

$$C_{\ell_1\ell_2} = \epsilon_{z_0} \times (\epsilon_{\mathrm{trg}_1} + \epsilon_{\mathrm{trg}_2} - \epsilon_{\mathrm{trg}_1}\epsilon_{\mathrm{trg}_2}) \times \mathrm{SF}_{\ell_1}\mathrm{SF}_{\ell_2}, \quad (4)$$

where ϵ_{z_0} is an event efficiency while $\epsilon_{\mathrm{trg}_i}$ and SF_{ℓ_i} are single lepton trigger efficiency and identification efficiency scale factors, respectively. The factor ϵ_{z_0} accounts for the efficiency of ± 60 cm cut on the z position of the reconstructed event vertex. By using a sample of minimally biased inelastic interactions, we find that this cut accepts $96.63 \pm 0.04(\mathrm{stat})\%$ of the full CDF luminous region. The lepton trigger efficiencies $\epsilon_{\mathrm{trg}_i}$ are measured in data samples selected with independent sets of triggers and found to be around 90% or better. Finally, the scale factors SF_{ℓ_i} are calculated as ratios of lepton identification efficiencies measured in data and in Monte Carlo simulations.

Table I lists all the factors used in the acceptance correction. Their central values are the luminosity weighted averages over different data taking periods, and the quoted uncertainties are only statistical. Using these as inputs to Eq. (4), we obtain values ranging from 73% to 93% for the correction factors $C_{\ell_1\ell_2}$, as shown in Table II, and a total denominator (1) for the 2.8 fb^{-1} DIL cross section of 19.43 ± 0.10 pb^{-1}, where the uncertainty comes solely from the propagation of the statistical uncertainties of each term in Eqs. (3) and (4).

B. Check of acceptance corrections

As a cross-check of our acceptance correction procedure, we calculate the cross section for Z production for each dielectron and dimuon category used in the DIL selection. With this check we verify the consistency of the correction procedure across the different dilepton categories.

We select events with ee or $\mu\mu$ in the final state and require the two leptons to have opposite charges and invariant mass in the range to 76–106 GeV/c^2. We follow the same lepton pairing used for the DIL dilepton selection. Cosmic ray induced events and events with an identified conversion are removed following the same criteria used for the $t\bar{t}$ dilepton selection. The number of events selected by these cuts is shown in Table III.

We use $Z/\gamma^* \to ee$ and $Z/\gamma^* \to \mu\mu$ PYTHIA Monte Carlo simulated samples to calculate the raw acceptance of the selection described above in the invariant mass $76\ \mathrm{GeV}/c^2 < M_{\ell\ell} < 106\ \mathrm{GeV}/c^2$. We use a formulation for the Z cross section calculation analogous to the $t\bar{t}$ cross section formulation in Eq. (1). In particular we employ the same factorization for the denominator correction calculation prescribed in the previous section by Eqs. (2)–(4).

We perform two checks: time independence of the acceptance correction factor for each DIL category and consistency of the correction procedure among different categories. With these checks we are not trying to measure the Z cross section but rather to determine if our understanding of the acceptance is correct. The Z cross section

TABLE I. Event vertex reconstruction efficiency ϵ_{z_0} and list, by lepton type, of trigger efficiency ϵ_{trg}, and lepton identification efficiency scale factors (SF) defined in Eq. (4). These are the luminosity weighted averages of efficiencies calculated for different data taking periods.

	Vertex reconstruction efficiency, ϵ_{z_0}
	0.9663 ± 0.0004
Lepton type	**Trigger efficiency, ϵ_{trg}**
CEM	0.965 ± 0.001
CMUP	0.917 ± 0.002
CMX	0.896 ± 0.002
	Lepton identification scale factor, SF
CEM	0.987 ± 0.001
PHX	0.932 ± 0.002
CMUP	0.927 ± 0.002
CMX	0.973 ± 0.002
CMU	0.97 ± 0.01
CMP	0.90 ± 0.01
CMIO	0.99 ± 0.01

TABLE II. List, by dilepton category, of raw acceptance $\mathcal{A}_{\ell_1\ell_2}$, correction factor $C_{\ell_1\ell_2}$, and luminosity $\mathcal{L}_i$ used in the calculation of the denominator for the 2.8 fb^{-1} DIL cross section measurement. The acceptance of each category includes contributions from nonisolated loose leptons. The $\mathcal{A}_{\ell_1\ell_2}$ uncertainty comes only from the MC statistics. The error in the $C_{\ell_1\ell_2}$ comes from the propagation of the dilepton efficiency uncertainties of Table I.

DIL category	$\mathcal{A}_{\ell_1\ell_2}(\%)$	$C_{\ell_1\ell_2}$	$\mathcal{L}_i(\mathrm{pb}^{-1})$
CEM-CEM	0.1224 ± 0.0017	0.9338 ± 0.0019	2826
CEM-PHX	0.0470 ± 0.0010	0.8658 ± 0.0027	2676
CMUP-CMUP	0.0498 ± 0.0011	0.8189 ± 0.0025	2826
CMUP-CMU	0.0191 ± 0.0007	0.7920 ± 0.0040	2826
CMUP-CMP	0.0267 ± 0.0008	0.7299 ± 0.0035	2826
CMUP-CMX	0.0474 ± 0.0010	0.8569 ± 0.0020	2760
CMUP-CMIO	0.0234 ± 0.0007	0.8050 ± 0.0040	2826
CMX-CMX	0.0106 ± 0.0005	0.8996 ± 0.0027	2760
CMX-CMU	0.0075 ± 0.0004	0.8134 ± 0.0043	2760
CMX-CMP	0.0115 ± 0.0005	0.7495 ± 0.0037	2760
CMX-CMIO	0.0101 ± 0.0005	0.8267 ± 0.0043	2760
CEM-CMUP	0.1769 ± 0.0020	0.8737 ± 0.0018	2826
CEM-CMU	0.0349 ± 0.0009	0.8879 ± 0.0040	2826
CEM-CMP	0.0475 ± 0.0010	0.8182 ± 0.0035	2826
CEM-CMX	0.0845 ± 0.0014	0.9171 ± 0.0019	2760
CEM-CMIO	0.0410 ± 0.0010	0.9025 ± 0.0041	2826
PHX-CMUP	0.0327 ± 0.0009	0.7723 ± 0.0029	2676
PHX-CMX	0.0147 ± 0.0006	0.7922 ± 0.0032	2623

TABLE III. Number of selected events and Z cross section in 2.8 fb^{-1} for the different ee and $\mu\mu$ dilepton categories with dilepton invariant mass in the range 76–106 GeV/c^2. Results are given both for the original and the fitted Z cross sections. The cross section uncertainties are only from the data statistics and from the propagation of the uncertainty in the single lepton efficiency of Table I.

Category	Number of events	Z Cross section (pb) original	Fitted
CEM-CEM	50 519	248.0 ± 1.4	248.0 ± 1.4
CEM-PHX	51 468	250.3 ± 1.4	250.3 ± 1.4
CMUP-CMUP	14 096	251.2 ± 2.4	251.2 ± 2.4
CMUP-CMU	5914	261.4 ± 3.7	243.8 ± 4.5
CMUP-CMP	6944	244.3 ± 3.2	250.1 ± 4.2
CMUP-CMX	20 007	247.1 ± 2.0	247.1 ± 2.0
CMUP-CMIO	9099	229.2 ± 2.7	240.3 ± 3.6
CMX-CMX	5563	250.8 ± 3.6	250.8 ± 3.6
CMX-CMU	3969	275.5 ± 4.7	257.0 ± 5.3
CMX-CMP	4280	241.8 ± 3.9	247.6 ± 4.8
CMX-CMIO	5771	251.0 ± 3.6	263.2 ± 4.4

has been independently measured by CDF as $\sigma_Z = 256 \pm 16$ pb [15].

For the first check, we look for possible time variations of the measured Z cross section in different data taking periods corresponding to integrated luminosities between 200 and 500 pb^{-1}. Figure 1 shows the result of these checks for dielectron channels. The error bar in the figure reflects uncertainties of data statistics, Monte Carlo statistics, and the acceptance correction procedure. We do not observe any systematic trend in the time dependence of the cross section for dielectron categories. The same conclusions hold for the dimuons channels. As an example, Fig. 2 shows the Z cross section time dependence for events with two tight muons.

For the second check, Table III reports the cross sections measured over the whole 2.8 fb^{-1} data sample for each dilepton category, using the efficiencies and scale factors of Table I. The categories with two tight leptons (CEM-CEM, CEM-PHX, CMUP-CMUP, CMUP-CMX, and

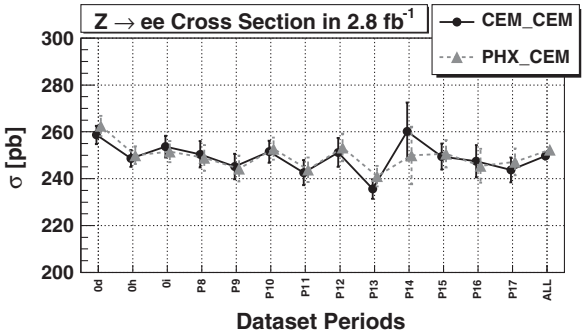

FIG. 1. Z cross section using dilepton categories with two electrons as a function of data taking period.

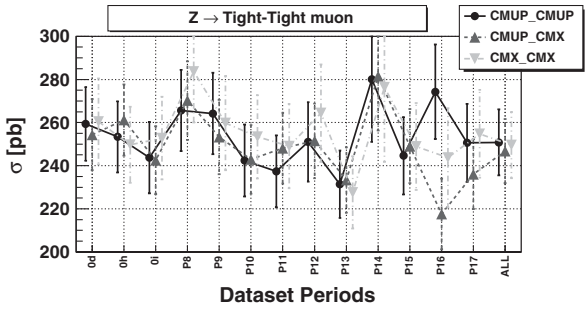

FIG. 2. Z cross section using dilepton categories with tight muons as a function of data taking period.

CMX-CMX), which are also the ones with the largest acceptance, are consistent with the theoretical prediction of $251.6^{+2.8}_{-3.1}$ pb [15]. Categories with a loose muon (CMP, CMU, or CMIO) paired to a tight muon show some residual variation around the average value which is not consistent with statistical fluctuations. In order to find a consistent normalization for all data, we perform a fit to the Z cross sections in the different dilepton categories with three free parameters, corresponding to a multiplicative factor in front of the selection efficiency of each of the three loose muon categories. The fit returns the cross sections reported in the last column of Table III and an average Z peak cross section of 249.1 ± 0.8 pb, as shown in Fig. 3. The Z peak cross section measured here does not include the 6% uncertainty in the luminosity which is common to all channels and which is the dominant uncertainty for the σ_Z measured in [15]. The free parameters returned by the fit are $SF^Z_{CMP} = 0.977 \pm 0.011$, $SF^Z_{CMU} = 1.072 \pm 0.011$, and $SF^Z_{CMIO} = 0.954 \pm 0.010$. They are folded into the acceptance correction procedure as additional scale factors to be multiplied by the lepton identification scale factors of Table I for the appropriate categories. After the fit, the single Z cross section

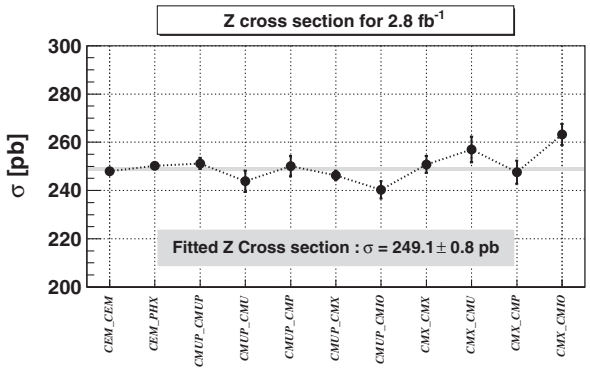

FIG. 3. Z peak cross section measured for each inclusive same flavor dilepton category using the full 2.8 fb^{-1} data sample after applying the loose muon scale factor. Not included is a 6% uncertainty in the luminosity measurement common to all channels. The band represents the mean value of 249.1 ± 0.8 pb.

measurements are consistent with each other within uncertainties, with the possible exception of categories containing one CMIO loose muon for which we observe a maximum deviation equal to 10% of the average value. This systematic deviation affects only 10% of the DIL $t\bar{t}$ raw acceptance, corresponding to the summed contributions of any dilepton pair containing a CMIO muon in Table II. Therefore, we estimate a final 1% systematic uncertainty on the acceptance due to the correction procedure.

V. BACKGROUNDS

We consider four different sources of standard model processes that can mimic the signature of dilepton plus $\not\!\!E_T$ plus 2 or more jets signature: diboson events (WW, WZ, ZZ, or $W\gamma$), Drell-Yan production of tau leptons (DY $\rightarrow \tau\tau$), Drell-Yan production of electrons or muons with additional $\not\!\!E_T$ (if the event is an actual Drell-Yan event, there is no $\not\!\!E_T$ so we refer to this as fake $\not\!\!E_T$) (DY $\rightarrow ee/\mu\mu$), and QCD production of W boson with multiple jets in which one jet is misidentified as a lepton (''W + jet fakes''). The two dominant sources of background are DY $\rightarrow ee/\mu\mu$ and W + jet fakes. These two processes have production cross sections much larger than the $t\bar{t}$, but they can only contaminate the $t\bar{t}$ dilepton signature of two leptons plus jets and large $\not\!\!E_T$ when misreconstructions of the event create either some large fake $\not\!\!E_T$ or a jet misidentified as a lepton. Because it is difficult to use the Monte Carlo simulation to predict the effect of event misreconstruction in our detector, we estimate the background from these two processes using data-based methods, as discussed in Secs. V A and V B, respectively. The diboson and DY $\rightarrow \tau\tau$ backgrounds are calculated using Monte Carlo simulation expectation as described in Secs. V C and V D. Corrections are applied for trigger and lepton ID efficiencies following the same procedure described in Sec. IV A.

Our strategy for validating the background estimation is to compare data and background estimates in the 0-jet and 1-jet bins, as discussed in Sec. VII.

A. W + jet fakes

Events with a single W boson plus jets can simulate the dilepton signature when one of the jets is misidentified as a lepton. The W + jet fake contamination is calculated in two steps: first we extract the probability of generic QCD jets faking the signatures of different lepton categories; then we apply these probabilities to weight events in the data containing one and only one high p_T lepton plus jets.

The fake probabilities are measured in generic jets from QCD decays by selecting ''fakeable'' leptons, which are jets passing minimal lepton identification criteria described below. We do not consider separately the heavy-flavor contribution to our backgrounds because the probability for a b or c quark to become a well-reconstructed high p_T lepton is very small. We define different categories of fakeable leptons, one per high p_T lepton category in the DIL dilepton selection.

Jets with a large fraction of neutral to charged pion production can create signatures with low track multiplicity and large energy deposition in the electromagnetic calorimeter, thus faking the presence of electrons. We define fakeable electrons as tracks of $p_T > 20$ GeV/c pointing to an electronlike cluster with energy deposition in the electromagnetic section of the calorimeter far exceeding the energy measured in the hadronic section, namely, with $E_{\mathrm{HAD}}/E_{\mathrm{EM}} < 0.125$. Fakeable electrons are further divided into objects that can fake CEM or PHX electrons depending on whether their clusters belong to the central or plug section of the calorimeter. We label them TCEM and TPHX, respectively. Fakeable for the nonisolated electrons do not require isolation for the central cluster and are called NCEM.

Jets whose full hadronic activity is limited to single charged pions or kaons with a late shower development or decay in flight might deposit little energy in the calorimeter but generate hits in the muon chambers, thus faking the signature of a muon. We define fakeable muons as good quality tracks of $p_T > 20$ GeV/c with $E/p < 1$. Depending on which muon subdetectors these tracks point to, we label as TCMUP, TCMX, LMIO, and LMUO fakeable muons which can fake tight CMUP, tight CMX, loose CMIO, or loose CMU/CMP muons, respectively. Fakeable muons that fail the isolation requirement are put together into a single NMUO category as long as they point to any muon subdetector.

We select fakeable leptons among generic QCD jets collected in four different control samples, whose main trigger requirement is the presence of at least one jet of $E_T^{\mathrm{Trg}} > 20$, 50, 70, and 100 GeV, respectively. The simplification of the jet algorithm used in these trigger selections tends to underestimate the energy of the offline reconstructed jets. To ensure a trigger efficiency of 90% or greater we require the trigger jet to have reconstructed E_T greater than 35, 55, 75, and 105 GeV, respectively, in the four jet samples. The resulting probabilities are labeled Jet20, Jet50, Jet70, and Jet100 fake lepton probabilities. To minimize real lepton contamination, we require that fakeables in the denominator of the fake probability fail one or more of the standard lepton identification cuts. For the numerator instead we require that the fakeable leptons pass all of the lepton identification requirements. We estimate the contamination of real leptons from W's, Drell-Yan, or dibosons, using Monte Carlo simulation predictions for the number of events with one lepton and at least one jet above the E_T threshold.

We use the fake lepton probability measured in the Jet50 sample as our primary estimator to apply to data events because the jet energy spectrum in the Jet50 sample is the

closest to the energy spectrum of jets in the dilepton plus missing E_T sample. The fake probabilities for different lepton categories show a dependence on the transverse energy of the fakeable lepton. To properly account for the difference in the p_T spectrum of fakeable leptons in QCD jets vs W + jets, we calculate fake probabilities in six p_T ranges as shown in Table IV.

The uncertainties on the fake probabilities in Table IV are only statistical. Variations in fake probabilities between the different QCD jet samples are used to estimate a systematic uncertainty in the lepton fake estimate. Figure 4 shows a comparison between the number of fake lepton events observed in the Jet20, Jet70, and Jet100 data sample, after integration over the full p_T spectrum, and the number predicted by the Jet50 fake probabilities of Table IV. We assess a 30% systematic uncertainty on the ability of the Jet50 fake probabilities to predict electron and muon fake contamination in samples with a wide range of jet energy.

We define ''lepton + fakeable'' as those events in the central high p_T lepton data sets with one and only one good high p_T lepton, $\not\!\!E_T > 25$ GeV and a second fakeable object failing at least one standard lepton identification cut. The fakeable object, which can be from any of the fakeable categories defined above, is paired to the good lepton and treated as the second lepton in the event when calculating any of the kinematic variables used in the top quark DIL selection, such as dilepton invariant mass, corrected $\not\!\!E_T$, and H_T. Jets found in a cone of $\Delta R < 0.4$ around the fakeable lepton are not included in the jet multiplicity count of that event because those jets are associated with the fake lepton in this W + jet fake estimation scheme. The fake lepton contamination is calculated by weighting each ''lepton + fakeable'' event found in data by the fake probability in Table IV. If more than one fakeable object is found in the event, we pair each of them to the good lepton and add their single fake contributions. The fake dilepton background thus calculated contains a statistical component, which is the sum of the fake probability uncertainty itself and the statistics of the ''lepton + fakeable'' sample.

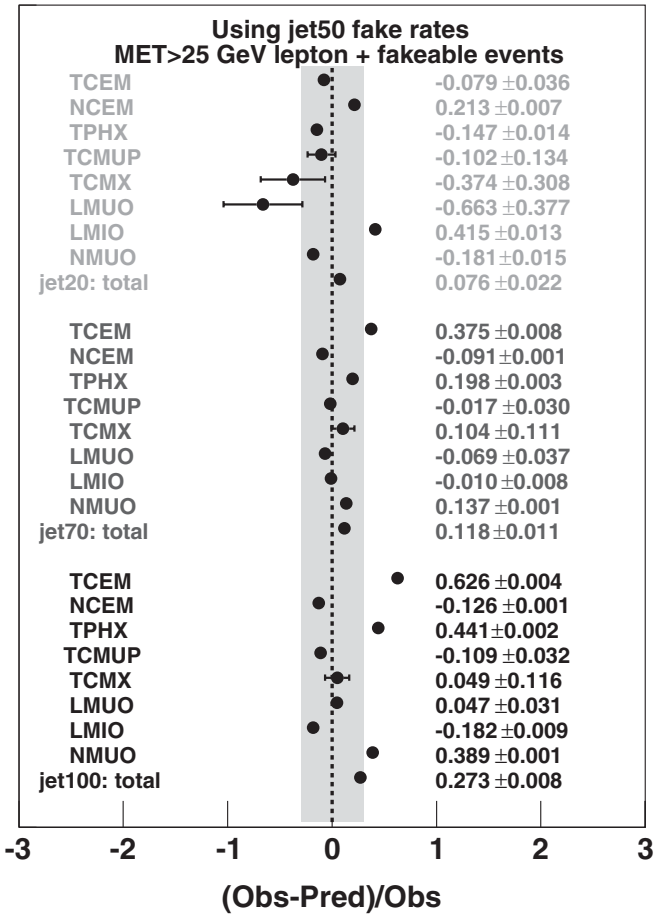

FIG. 4. Ratio of observed total number of fake leptons for each fakeable category vs the Jet50-based prediction normalized by the number of observed fake leptons. The predictability of the jet50 P_T dependent fake rate is good at the 30% level, as shown by the band in the plot. When error bars are not shown they are smaller than the dot size.

As a check, we compare the same sign ''lepton+ fakeable'' prediction to the number of W + jet fakes with same sign dilepton candidates in the signal regions. We define as fake lepton charge the charge of the track

TABLE IV. Jet50 fake probabilities vs fakeable lepton p_T for different fakeable categories. The uncertainties are statistical only. Because of the definition of fake probability, the denominator can fluctuate to be smaller than the numerator in low statistics high p_T bins, hence fake rate values exceeding 100%.

Jet50 fake probabilities (%) in p_T range (GeV/c)						
Fakeable	[20–30]	[30–40]	[40–60]	[60–100]	[100–200]	≥ 200
TCEM	4.97 ± 0.09	3.68 ± 0.08	2.39 ± 0.01	2.88 ± 0.02	3.26 ± 0.11	4.98 ± 3.44
NCEM	0.74 ± 0.1	0.53 ± 0.01	0.58 ± 0.01	0.49 ± 0.01	0.80 ± 0.07	—
TPHX	12.6 ± 0.1	13.9 ± 0.1	12.7 ± 0.1	20.4 ± 0.2	26.8 ± 0.2	65.0 ± 57.3
TCMUP	0.99 ± 0.04	2.30 ± 0.10	3.82 ± 0.14	6.30 ± 0.28	4.13 ± 0.47	—
TCMX	0.91 ± 0.06	2.20 ± 0.15	4.74 ± 0.21	5.09 ± 0.55	0.76 ± 1.98	0.44 ± 0.25
LMUO	2.48 ± 0.05	2.88 ± 0.14	4.41 ± 0.23	5.45 ± 0.47	7.51 ± 0.64	0.41 ± 0.26
LMIO	21.0 ± 0.1	25.4 ± 0.3	27.8 ± 0.4	40.1 ± 0.1	37.0 ± 1.5	107.1 ± 14.8
NMUO	0.51 ± 0.01	0.36 ± 0.01	0.23 ± 0.01	0.25 ± 0.01	0.29 ± 0.04	0.17 ± 0.18

associated to the fakeable lepton. Same sign dilepton candidates are corrected for the presence of same sign pairs coming from $t\bar{t}$, DY, or diboson events that are simulated in our Monte Carlo simulations. The results of this check are shown in Table V. Although the $\mu\mu$ channel shows deviation at the 3 standard deviation level for some jet multiplicity bins, the agreement in the final predictions over all dilepton categories is at the 1 standard deviation level.

B. Drell-Yan to $ee/\mu\mu$ background

The contamination from $Z/\gamma^* \rightarrow ee/\mu\mu$ decays is calculated using a combination of data-based and MC-based predictions. We define DIL data samples enriched in DY events after the L-cut by inverting the Z-veto cut and extrapolating the remaining DY contamination in the signal region by using the relative contribution of $Z/\gamma^* \rightarrow ee/\mu\mu$ decays passing and failing the Z-veto cut as predicted from MC. The Z-veto cut (see Sec. III) requires that the dilepton invariant mass be outside the Z window region of 76–106 GeV$/c^2$, or, if inside, that the event have missing E_T significance $\not\!\!E_T/\sqrt{E_T^{\rm sum}} > 4$ GeV$^{(1/2)}$.

We calculate the DY $\rightarrow ee/\mu\mu$ contamination as the sum of two contributions, one outside the Z window region, $N_{\rm out}$, and one inside the Z window with high MetSig, $N_{\rm high}$. The first contribution is calculated as

$$N_{\rm out} = R_{\rm out/in}(N_{\rm in}^{\rm DT} - N_{\rm in}^{\rm BKG}), \quad (5)$$

where $N_{\rm in}^{\rm DT}$ and $N_{\rm in}^{\rm BKG}$ represent the number of events inside the Z-window passing the L-cut in data and in non-DY MC background predictions, respectively. $R_{\rm out/in}$ is the ratio of $Z/\gamma^* \rightarrow ee/\mu\mu$ events outside to inside the Z window predicted by the ALPGEN [16] Monte Carlo generator.

The second contribution is calculated as

$$N_{\rm high} = R_{\rm high/low}(N_{\rm low}^{\rm DT} - N_{\rm low}^{\rm BKG}), \quad (6)$$

where $N_{\rm low}^{\rm DT}$ and $N_{\rm low}^{\rm BKG}$ represent the events inside the Z-window passing the L-cut with MetSig < 4 GeV$^{(1/2)}$ for data and for non-DY MC background predictions, respectively. $R_{\rm high/low}$ is the ratio of events passing/failing the MetSig > 4 GeV$^{(1/2)}$ cut predicted by ALPGEN. Table VI summarizes the inputs to Eqs. (5) and (6) and the final values of $N_{\rm out}$ and $N_{\rm high}$ for each jet multiplicity bin. For the calculation of $t\bar{t}$ contribution to $N^{\rm BKG}$ we use the prediction of 6.7 pb for the cross section. We later correct this iteratively to the value measured in the data.

The DY contamination in the signal sample is extracted from the $N_{\rm out}$ and $N_{\rm high}$ estimates in the ≥ 2 jet bin, corrected for the efficiency of the $H_T > 200$ GeV and of the opposite sign lepton cuts. The combined efficiency for these two cuts is calculated using ALPGEN simulated Z samples and shown as $\epsilon_{\rm OS}$ in Table VII.

The contamination of $Z/\gamma^* \rightarrow \mu\mu$ to $e\mu$ events comes mostly from cases where one of the final state muon

TABLE V. Comparison between the same sign dilepton fake background prediction using the fake rate tables and the numbers of same sign dilepton candidates found in the signal region, after MC subtraction of standard model contamination sources.

Number of SS dilepton events	ee	$\mu\mu$	$e\mu$	All
Corrected candidates in 0 jet	13.0 ± 4.4	11.3 ± 3.7	14.8 ± 5.0	39.0 ± 7.6
Predicted candidates in 0 jet	8.1 ± 2.6	7.8 ± 2.7	18.0 ± 5.6	33.9 ± 10.4
Corrected candidates in 1 jet	7.8 ± 3.5	0.5 ± 1.4	24.9 ± 5.6	33.2 ± 6.7
Predicted candidates in 1 jet	5.1 ± 1.6	6.9 ± 2.2	25.4 ± 7.8	37.3 ± 11.4
Corrected candidates in 2 or more jets	5.0 ± 2.7	0.7 ± 1.0	24.7 ± 5.2	30.4 ± 5.9
Predicted candidates in 2 or more jets	3.8 ± 1.2	7.5 ± 2.4	24.5 ± 7.6	35.9 ± 11.0

TABLE VI. Inputs to Eqs. (5) and (6) and for each dilepton flavor and jet multiplicity. $N_{\rm out}$ and $N_{\rm high}$ are the final values of the DY $\rightarrow ee$ and $\mu\mu$ background contamination outside the Z peak region and inside the Z peak region with high MetSig, respectively.

	0-jet		1-jet		$\geq$ 2-jets	
	ee	$\mu\mu$	ee	$\mu\mu$	ee	$\mu\mu$
$N_{\rm in}^{\rm DT}$	78	45	76	58	73	43
$N_{\rm in}^{\rm BKG}$	29.6 ± 1.4	20.1 ± 1.0	16.5 ± 1.6	11.9 ± 1.4	17.0 ± 1.2	16.8 ± 1.0
$R_{\rm out/in}$	0.39 ± 0.05	0.45 ± 0.09	0.31 ± 0.05	0.31 ± 0.06	0.32 ± 0.02	0.26 ± 0.02
$N_{\rm out}$	19.1 ± 3.7	11.3 ± 3.2	18.2 ± 2.8	14.2 ± 2.5	18.2 ± 2.8	6.8 ± 1.7
$N_{\rm low}^{\rm DT}$	65	37	69	54	65	39
$N_{\rm low}^{\rm BKG}$	12.6 ± 0.7	9.5 ± 0.6	5.9 ± 0.5	5.5 ± 0.5	6.7 ± 0.2	8.0 ± 0.5
$R_{\rm high/low}$	0.026 ± 0.009	0.010 ± 0.005	0.049 ± 0.006	0.049 ± 0.011	0.040 ± 0.003	0.040 ± 0.004
$N_{\rm high}$	1.23 ± 0.21	0.26 ± 0.06	2.85 ± 0.41	2.34 ± 0.36	2.16 ± 0.32	1.22 ± 0.25

TABLE VII. H_T and opposite sign cut efficiency for the DY $\rightarrow$ ee and $\mu\mu$ background contamination in ≥ 2 jet region. The efficiency is calculated separately for events outside the Z peak region passing the L-cut, and for events inside the Z peak region also passing the MetSig > 4 GeV$^{(1/2)}$ cut.

$\epsilon_{H_T,\mathrm{OS}}$	ee	$\mu\mu$
For N_{out} events	0.54 ± 0.03	0.60 ± 0.05
For N_{in} events	0.95 ± 0.01	0.99 ± 0.01

radiates a very energetic photon. These photons, which are almost collinear to the muon, deposit their energy in the EM calorimeter and produce a cluster which is associated with the original muon track and fakes the electron signature. The missed muon gives rise to a sizable $\not\!\!E_T$ in the event, curtailing the effectiveness of the L-cut and Z-veto to reject them. As no data-based control sample is available for this contamination, we estimate it using Monte Carlo simulation predictions.

C. Diboson background

The diboson processes, WW, WZ, ZZ, and $W\gamma$, can mimic the signature of the $t\bar{t}$ signal via different mechanisms, with real leptons and $\not\!\!E_T$ from W and Z decays and jets produced by boson hadronic decays or initial and final state radiation. For WW events, the two leptons and the $\not\!\!E_T$ are produced when both W's decay semileptonically but the jets require some hadronic radiation external to the diboson system. For WZ and ZZ events, the two leptons come from the Z boson while the other W or Z boson provides the jets via their hadronic decays. As these decays do not contain any neutrino, some mechanism is required to produce fake missing transverse energy. Finally for $W\gamma$ events, one lepton plus $\not\!\!E_T$ is generated from the semileptonic W decay while the second lepton is produced from an asymmetric γ conversion in which one of the two electrons has little energy and is caught spiralling inside the central drift chamber. Like in the WW case, the $W\gamma$ system is accompanied by hadronic jets. Events involving W + jets fake leptons, with a real lepton from the W boson paired to a fake lepton from the hadronic decays of the other boson, are removed from the MC to avoid double counting.

Only WW background contribute to the ee, $\mu\mu$, and $e\mu$ final states in the same proportion as the $t\bar{t}$ signal. Diboson processes involving a Z contribute preferentially to the same flavor lepton categories. $W\gamma$ events do not contribute any background to the $\mu^+\mu^-$ category given the negligible probability that the photon will convert to a muon pair.

The WW, WZ, and ZZ processes are simulated with the PYTHIA Monte Carlo generator. Their production cross section is taken from the latest next-to-leading order (NLO) MCFM (a Monte Carlo for FeMtobarn processes at Hadron colliders) version [17] and CTEQ6 [18] parton distribution function predictions to be $\sigma_{WW} = 12.4 \pm 0.8$ pb, $\sigma_{WZ} = 3.7 \pm 0.1$ pb. For the ZZ events, a cross section $\sigma_{ZZ} = 3.8$ pb is assumed with an uncertainty of 20%. $W\gamma$ decays are simulated with the BAUR Monte Carlo generator [19]. The leading order (LO) production cross section of $\sigma_{W\gamma} = 32 \pm 3$ pb is assumed and multiplied by a K-factor of 1.36 [20] to correct for NLO effects. The $W\gamma$ Monte Carlo generator acceptance prediction is multiplied by a conversion inefficiency scale factor of 1.15 ± 0.35 to correct for the imperfect simulation of the tracking variables used in the conversion identification algorithm.

Monte Carlo generators do not correctly model the jet production from hadronic radiation, as is seen by comparing the jet multiplicity spectra of data and MC predictions for ee and $\mu\mu$ events in the Z peak region. Data, even after correcting the jet multiplicity spectrum for other SM contributions, have higher fractions of events in the 2 or more jet bins compared to predictions. We calculate jet multiplicity scale factors C_{Nj} as ratios of data and MC events in each jet bin, after normalizing the MC to the number of data in the Z peak region. These scale factors, shown in Table VIII, are used to correct the jet multiplicity of WW and $W\gamma$ events. A 5% systematic uncertainty on this correction is assessed by comparing jet multiplicity scale factors calculated with different generators.

D. Drell-Yan $\rightarrow \tau\tau$ background

$Z/\gamma^* \rightarrow \tau^+\tau^-$ decays are simulated with the ALPGEN generator. These events can fake the dilepton plus $\not\!\!E_T$ plus 2 or more jets signature when both τ's decay semileptonically to $\ell^+\nu_\ell\bar{\nu}_\tau\ell^-\bar{\nu}_\ell\nu_\tau$ and jets from initial and final state radiation are present. The contamination from this process is expected to contribute equally to the e^+e^- and $\mu^+\mu^-$ categories and to be twice as big in the $e^\pm\mu^\mp$ channel. The neutrinos from the semileptonic τ decays tend to have lower energy than the neutrinos in the $t\bar{t}$ dilepton sample and align along the direction of the leptonic decay when the Z recoils against the external jets. Hence a big fraction of the $Z/\gamma^* \rightarrow \tau\tau$ events are removed by the L-cut, the cut on the event $\not\!\!E_T > 25$ GeV or $\not\!\!E_T > 50$ GeV in case any lepton or jet is closer than 20° to the $\not\!\!E_T$ direction (see Sec. III).

TABLE VIII. Jet multiplicity scale factors for $Z \rightarrow e^+e^-$ and $Z \rightarrow \mu^+\mu^-$ events in the 0-jet bin (C_{0j}), 1-jet bin (C_{1j}), and $\geq$ 2-jet bin (C_{2j}), respectively. The last column is the weighted average of the two same flavor Z samples and it is used as the correction factor for $e\mu$ reconstructed events. The uncertainties shown here are statistical only.

	Jet multiplicity scale factor		
	e^+e^-	$\mu^+\mu^-$	$\ell^+\ell^-$
C_{0j}	1.017 ± 0.010	0.999 ± 0.011	1.010 ± 0.010
C_{1j}	0.918 ± 0.012	0.991 ± 0.012	0.948 ± 0.008
C_{2j}	1.056 ± 0.020	1.123 ± 0.020	1.082 ± 0.014

The final contamination from this process is estimated using a Monte Carlo simulation and assumes a $Z \rightarrow \tau\tau$ cross section of $251.6^{+2.8}_{-3.1}$ pb [15]. The simulated samples are generated using ALPGEN generator [16] that has built-in matching of the number of jets, coupled with PYTHIA [14] for the shower evolution, and EVTGEN [21] for the heavy-flavor hadron decays. All simulated events were run through the full CDF detector simulation. To correct for NLO effects, this value is further multiplied by a K-factor of 1.4 [22]. The MC predictions in the different jet bins are finally rescaled by the C_{Nj} scale factors, as discussed in Sec. V C.

VI. SYSTEMATIC UNCERTAINTIES

The systematic uncertainty for the cross section measurement has two main contributions: systematics in the $t\bar{t}$ dilepton acceptance and systematics in the background estimation. We distinguish between the uncertainties affecting only the signal or the background from the uncertainties common to both.

For the signal acceptance, we consider systematic uncertainties coming from different MC generators, different assumed amounts of initial (ISR) and final (FSR) state radiation in the PYTHIA Monte Carlo, calculated by comparing data to expectations for the p_T spectrum of the dilepton system in Drell-Yan events and for the kinematic distributions of the underlying events and different parton distribution functions. These sources are uncorrelated from each other. The two remaining and largest sources of acceptance systematics are common to signal and background Monte Carlo simulation predictions. They arise from uncertainties in the lepton identification (ID) scale factors and JES. Comparing the lepton ID scale factors calculated for Z events with 0, 1, and ≥ 2 jets, we derive a systematic uncertainty associated with the Monte Carlo generator acceptance correction of 2%. This is added in quadrature to the 1% systematic uncertainty on the acceptance correction procedure derived from measurement of the Z cross section in different dilepton channels (see Sec. IV A), for a total systematic uncertainty on the lepton ID correction of 2.2%. The JES uncertainty is calculated by measuring the shift in acceptance due to varying the jet energy scale correction applied to each jet in the event by ± 1 standard deviation of its systematic uncertainty. Table IX summarizes the systematic uncertainties in the $t\bar{t}$ acceptance separated by the contributions which are independent and contributions which are common with the systematic uncertainty in the background prediction. Common contributions affect both the numerator and the denominator of Eq. (1) used to calculate the final $t\bar{t}$ cross section. Their correlation is taken into account when calculating the systematic uncertainty on the measured $t\bar{t}$ cross section.

Uncorrelated sources of systematic uncertainties affecting the backgrounds are the 30% systematic uncertainty on the fakes contamination, the 30% uncertainty on the conversion inefficiency scale factor affecting the $W\gamma$ contamination, and the theoretical uncertainties, ranging from 2%–10%, on the production cross sections of diboson and $Z \rightarrow \tau\tau$ processes. Although large, each of these systematics affects only a fraction of the total background. Finally, a systematics common to most Monte Carlo generator predictions of background processes with jet production from QCD radiation comes from the 5% uncertainty in the C_{Nj} correction factors of Sec. V C.

TABLE IX. Summary of systematic uncertainties affecting the $t\bar{t}$ acceptance: The entries in the top part of the table are treated as uncorrelated and added in quadrature when calculating their contribution to $t\bar{t}$ cross section systematic uncertainty via the denominator of Eq. (1); the two entries in the bottom part of the table are also added in quadrature but their correlation with the systematic uncertainty in the background prediction, which appears in the numerator of Eq. (1), is taken into account when calculating the final systematic uncertainty in the $t\bar{t}$ cross section.

Source	Systematic error (%)
MC generator	1.5
ISR	1.7
FSR	1.1
PDF	0.8
Lepton ID	2.2
Jet corrections	3.2

VII. CONTROL SAMPLES

We use dilepton events passing both the L-cut and Z-veto cut, but with only 0 or 1 jets as control samples for the background calculation. The $t\bar{t}$ contamination to the 0 jet samples is negligible and the contribution to the 1 jet sample is small. The results for the number of observed and expected events in the various dilepton flavor categories are shown in Table X. The $t\bar{t}$ contribution has been calculated assuming a production cross section of 6.7 pb. For the 0-jet bin data, the single largest contribution is from diboson production, followed by W + jet fakes and DY production; for the 1-jet bin data the single largest contribution is from W + jet fakes, followed by diboson and DY production. Figures 5 and 6 show the 0-jet and 1-jet data overlaid on top of the background and $t\bar{t}$ predictions for four different kinematic distributions: single lepton p_T, dilepton invariant mass, event missing transverse energy $\not\!\!E_T$, and total scalar transverse energy H_T. The largest deviation, still below the 2 standard deviation level, is in the $N_{\text{jet}} = 0$ control sample for the $\mu\mu$ channel. Overall the data are in good agreement with the expectations of background plus signal ($t\bar{t}$). The agreement is quantified in terms of the probability for the χ^2/ndf distribution and shown as "χ^2 Test" on the figures.

TABLE X. Summary table, by lepton flavor content of background estimates, $t\bar{t}$ predictions, and observed events in data corresponding to an integrated luminosity of 2.8 fb^{-1} for the 0-jet (top) and 1-jet (bottom) bins, respectively. The quoted uncertainties are the sum of the statistical and systematic uncertainty.

$N_{jet} = 0$ control sample per dilepton flavor category				
Source	ee	$\mu\mu$	$e\mu$	$\ell\ell$
WW	36.36 ± 3.26	30.10 ± 2.71	76.40 ± 6.76	142.87 ± 12.57
WZ	2.88 ± 0.21	4.56 ± 0.31	4.21 ± 0.29	11.65 ± 0.74
ZZ	4.13 ± 3.19	4.25 ± 3.28	0.41 ± 0.32	8.79 ± 6.78
$W\gamma$	14.26 ± 4.90	0.00 ± 0.00	13.77 ± 2.63	28.03 ± 7.11
DY $\rightarrow \tau\tau$	0.95 ± 0.26	0.79 ± 0.23	2.15 ± 0.39	3.89 ± 0.58
DY $\rightarrow ee + \mu\mu$	20.32 ± 3.94	11.59 ± 3.34	8.13 ± 1.33	40.04 ± 5.77
W + jet fakes	18.72 ± 5.73	15.29 ± 4.93	38.47 ± 11.72	72.49 ± 19.02
Total background	97.64 ± 14.47	66.58 ± 9.23	143.54 ± 15.65	307.76 ± 35.84
$t\bar{t}$ ($\sigma = 6.7$ pb)	0.15 ± 0.03	0.18 ± 0.03	0.34 ± 0.04	0.67 ± 0.06
Observed	99	96	147	342

$N_{jet} = 1$ control sample per dilepton flavor category				
Source	ee	$\mu\mu$	$e\mu$	$\ell\ell$
WW	9.74 ± 1.08	8.73 ± 0.97	21.55 ± 2.31	40.01 ± 4.24
WZ	4.95 ± 0.25	2.66 ± 0.15	4.11 ± 0.21	11.72 ± 0.52
ZZ	1.59 ± 1.23	1.58 ± 1.22	0.91 ± 0.70	4.08 ± 3.14
$W\gamma$	3.70 ± 1.47	0.00 ± 0.00	4.43 ± 1.12	8.14 ± 2.27
DY $\rightarrow \tau\tau$	4.64 ± 0.83	4.42 ± 0.78	8.81 ± 1.50	17.87 ± 2.99
DY $\rightarrow ee + \mu\mu$	21.04 ± 4.27	16.48 ± 3.56	3.31 ± 0.90	40.83 ± 7.28
W + jet fakes	12.14 ± 3.73	14.84 ± 4.60	67.26 ± 20.43	94.23 ± 26.16
Total background	57.80 ± 8.97	48.70 ± 7.57	110.37 ± 21.27	216.87 ± 32.46
$t\bar{t}$ ($\sigma = 6.7$ pb)	3.94 ± 0.22	4.02 ± 0.22	9.47 ± 0.49	17.44 ± 0.86
Observed	58	54	107	219

VIII. $t\bar{t}$ USING 2 JET SELECTION

As an intermediate step toward the final result, Table XI shows the predictions for signal and background in events with two or more jets passing all of the $t\bar{t}$ selection criteria except the $H_T > 200$ GeV and the opposite lepton charge requirement. For this sample the $t\bar{t}$ signal contribution is almost equal to the total background contribution. There is good agreement between the predicted and observed number of events both in overall normalization and in the bin-by-bin distribution for the same four kinematic variables used in the 0- and 1-jet control samples, as shown in Fig. 7. The agreement is quantified in terms of the probability for the χ^2/ndf distribution and shown as "χ^2 Test" on the figures.

IX. RESULTS

The signal and background DIL candidate events, that is events in the 2 or more jet samples after the final $H_T > 200$ GeV and opposite charge requirements, are shown in Table XII separately for the different dilepton flavor contribution. The $t\bar{t}$ rate is computed assuming a $t\bar{t}$ production cross section in agreement with the NLO standard model calculation for a top mass of 175 GeV/c^2, of $6.7^{+0.7}_{-0.9}$ pb [3]. The sum of the background and signal contributions is labeled "Total SM expectation" and can be compared to the number of "Observed" data in 2.8 fb^{-1}. Figure 8 shows the $t\bar{t}$ and the different backgrounds overlaid on the data, for the single lepton p_T, dilepton invariant mass, the event $\not\!\!E_T$, and H_T distributions. Again there is overall good agreement between data and total background plus $t\bar{t}$ expectations, as shown by the probability for the χ^2/ndf distribution reported on the figures.

Table XIII summarizes the background and signal predictions for the 0, 1, and ≥ 2 jet bin control samples and for the signal sample. Figure 9 shows the overall number of candidate events in the different jet multiplicity bins overlaid on top of a stacked histogram of the different background components. The band gives the $t\bar{t}$ contribution for a cross section of 6.7 pb. The hatched area represents the uncertainty in the total background estimate. From the difference between the observed data and the total background predictions, we measure a cross section for $t\bar{t}$ events in the dilepton channel of

$$\sigma_{t\bar{t}} = 6.27 \pm 0.73(\text{stat}) \pm 0.63(\text{syst}) \pm 0.39(\text{lum}) \text{ pb},$$

where the first uncertainty is statistical, the second is the convolution of the acceptance and background

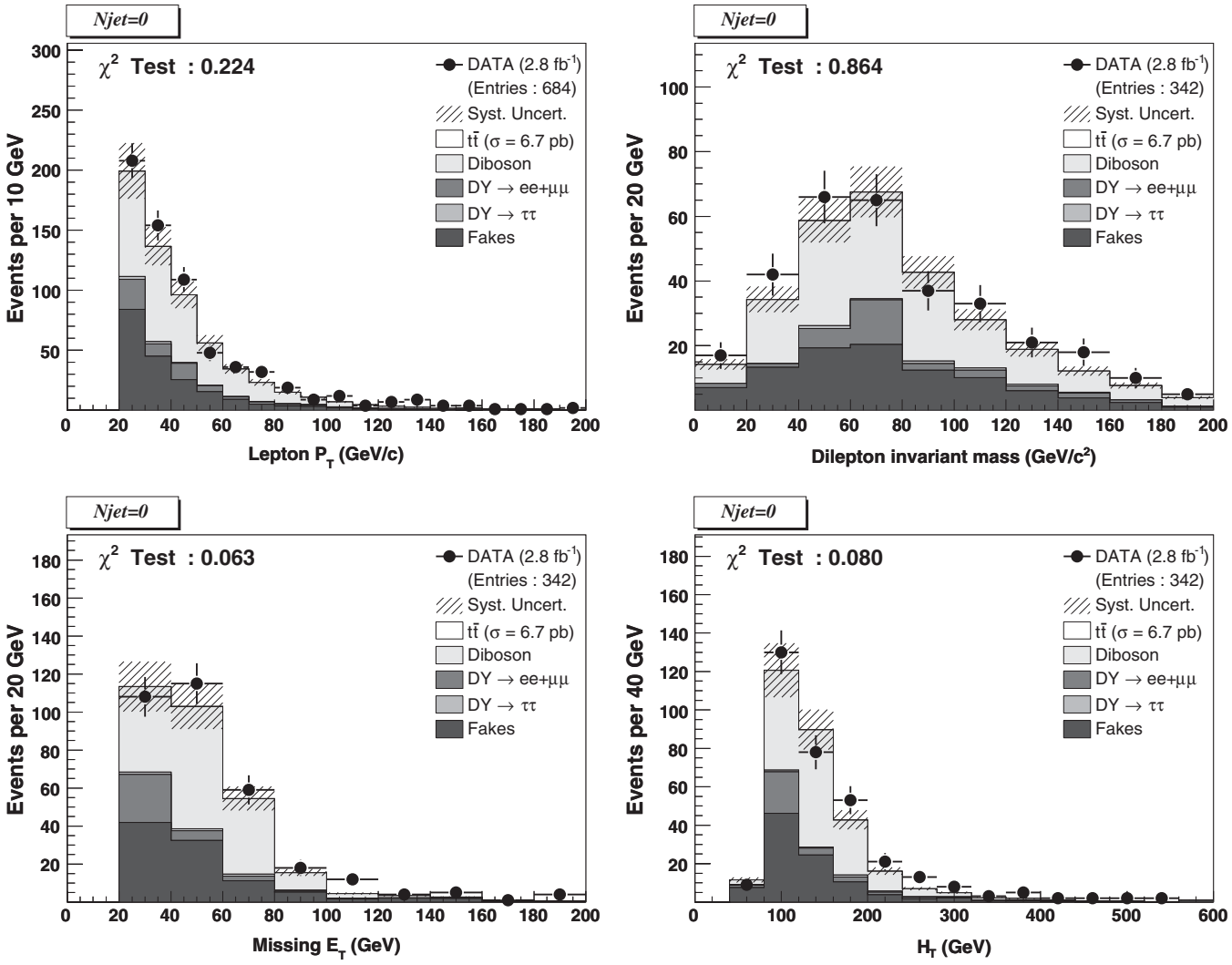

FIG. 5. Background and top quark signal predictions overlaid on the data for 0-jet events in 2.8 fb^{-1}. From top left to bottom right: two leptons transverse energy spectrum, the dilepton invariant mass, the event $\not\!\!E_T$ and H_T. The hatched area represents the uncertainty in the total background estimate.

systematics, and the third comes from the 6% uncertainty in the luminosity measurement. This result assumes a top quark mass of $M_t = 175\ \mathrm{GeV}/c^2$. Studies of the DIL selection acceptance vs M_t show an increase in acceptance of 3% for each $1\ \mathrm{GeV}/c^2$, in the range $\pm 2\ \mathrm{GeV}/c^2$ around the combined Tevatron top quark mass measurement of $M_t = 173.1 \pm 0.6_{\mathrm{stat}} \pm 1.1_{\mathrm{syst}}\ \mathrm{GeV}/c^2$ [23]. The theory cross section decreases by approximately 0.2 pb for each $1\ \mathrm{GeV}/c^2$ increase over the mass range from 170–180 GeV/c^2.

As a test of lepton universality, we quote the results for the individual dilepton flavor decay modes:

$$\sigma_{t\bar{t}}(ee) = 4.57 \pm 1.56(\mathrm{stat}) \pm 0.58(\mathrm{syst})\ \mathrm{pb}$$

$$\sigma_{t\bar{t}}(\mu\mu) = 7.47 \pm 1.63(\mathrm{stat}) \pm 0.79(\mathrm{syst})\ \mathrm{pb},$$

$$\sigma_{t\bar{t}}(e\mu) = 6.43 \pm 0.95(\mathrm{stat}) \pm 0.69(\mathrm{syst})\ \mathrm{pb}.$$

All of the results are consistent with each other. Similar conclusions hold for the cross section of signal events where both leptons are isolated, which is a sample extensively used in other SM precision measurements like the Z cross section measurement:

$$\sigma_{t\bar{t}}(\mathrm{iso}) = 6.40 \pm 0.75(\mathrm{stat}) \pm 0.49(\mathrm{syst})\ \mathrm{pb}.$$

The luminosity error is common to all of these subsamples and is not explicitly quoted.

X. CONCLUSIONS

We present a measurement of the $t\bar{t}$ cross section at the Tevatron in a sample of data corresponding to an integrated luminosity of 2.8 fb^{-1} collected by the CDF II detector. Using events with two leptons, large missing energy, and

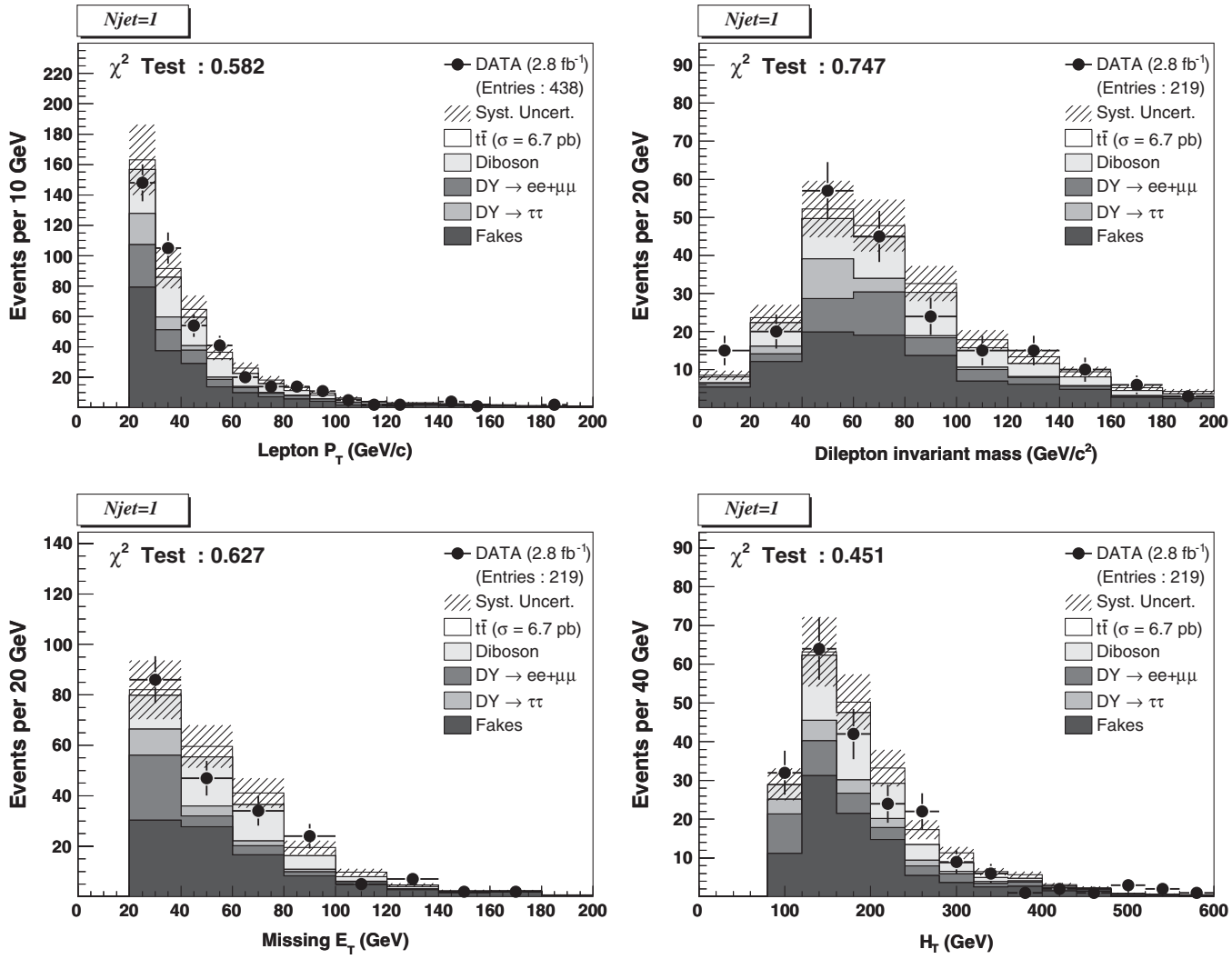

FIG. 6. Background and top quark signal predictions overlaid on the data for 1-jet events in 2.8 fb^{-1} From top left to bottom right: two leptons transverse energy spectrum, the dilepton invariant mass, the event $\not\!\!E_T$ and H_T. The hatched area represents the uncertainty in the total background estimate.

TABLE XI. Summary table by lepton flavor content of background estimates, $t\bar{t}$ predictions, and observed events in data corresponding to an integrated luminosity of 2.8 fb^{-1} for the ≥ 2 jet bin before the H_T and the opposite lepton charge requirement events. The uncertainties are the sums in quadrature of the statistical and systematic errors. The last column is the total dilepton sample obtained as the sum of the ee, $\mu\mu$, and $e\mu$ contributions.

$N_{jet} \geq 2$ $t\bar{t}$ sample per dilepton flavor category				
Source	ee	$\mu\mu$	$e\mu$	$\ell\ell$
WW	3.54 ± 0.63	3.65 ± 0.65	7.50 ± 1.28	14.70 ± 2.47
WZ	1.75 ± 0.23	1.01 ± 0.14	1.68 ± 0.23	4.44 ± 0.57
ZZ	0.83 ± 0.65	0.74 ± 0.58	0.47 ± 0.37	2.04 ± 1.59
$W\gamma$	0.62 ± 0.41	0.00 ± 0.00	1.45 ± 0.58	2.07 ± 0.78
DY $\rightarrow \tau\tau$	2.97 ± 0.75	3.29 ± 0.84	6.68 ± 1.67	12.94 ± 3.22
DY $\rightarrow ee + \mu\mu$	20.33 ± 6.00	8.04 ± 2.73	1.76 ± 0.72	30.13 ± 8.54
W + jet fakes	9.66 ± 3.00	18.67 ± 5.77	54.67 ± 16.59	83.00 ± 22.90
Total background	39.71 ± 8.73	35.40 ± 7.36	74.22 ± 17.13	149.33 ± 28.19
$t\bar{t}$ ($\sigma = 6.7$ pb)	31.25 ± 1.52	32.69 ± 1.59	74.62 ± 3.58	138.56 ± 6.61
Observed	58	68	143	269

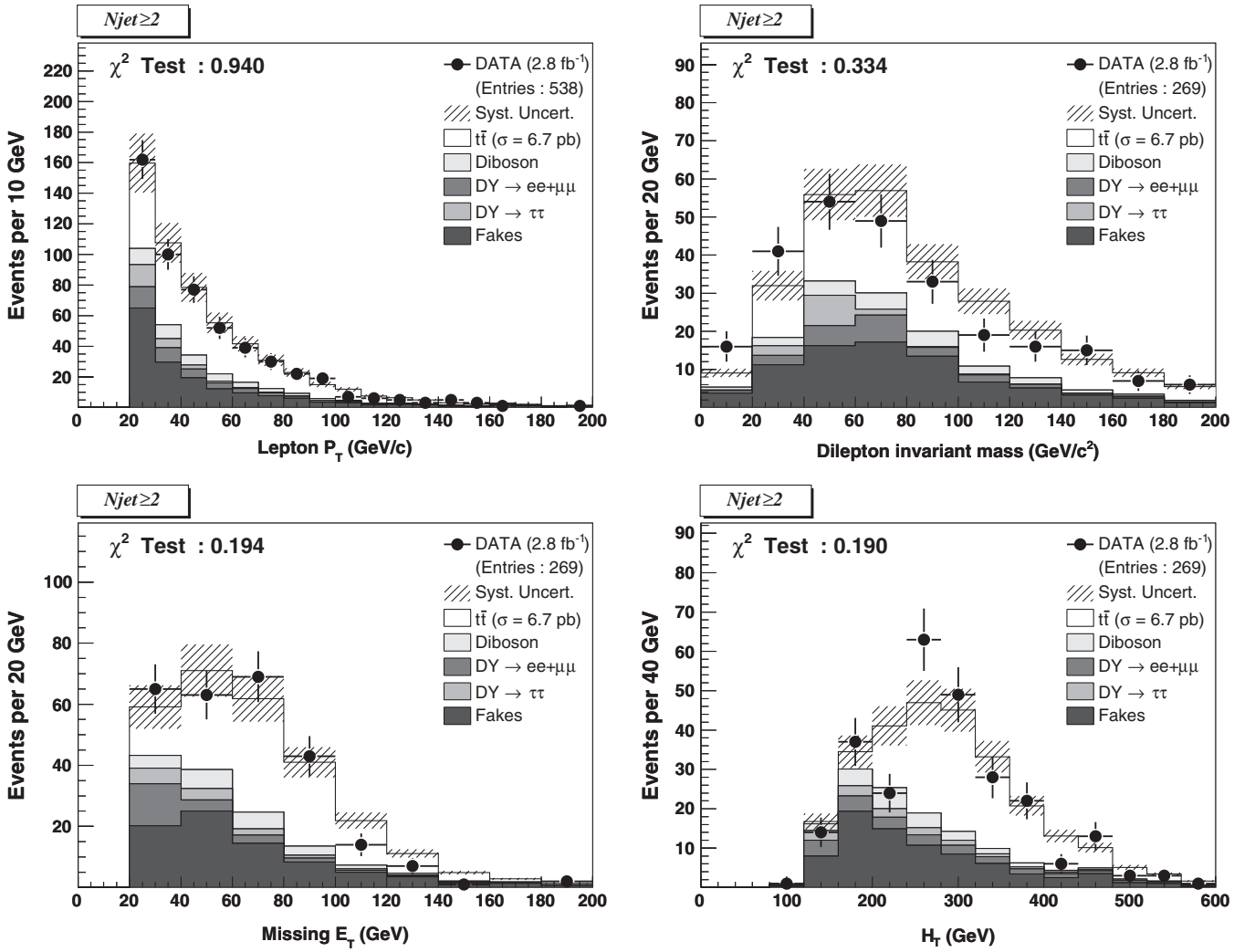

FIG. 7. Background and top quark signal predictions overlaid on the data for 2-jet events before the H_T and the opposite lepton charge requirement in 2.8 fb^{-1}. From top left to bottom right: Two leptons transverse energy spectrum, the dilepton invariant mass, the event $\not\!\!E_T$ and H_T. The hatched area represents the uncertainty in the total background estimate.

TABLE XII. Summary table by lepton flavor content of background estimates, $t\bar{t}$ predictions, and observed events in the final sample of events with ≥ 2 jets passing all candidate selection criteria, for an integrated luminosity of 2.8 fb^{-1}. The uncertainties are the sums in quadrature of the statistical and systematic errors. The last column is the total dilepton sample obtained as the sum of the ee, $\mu\mu$, and $e\mu$ contributions.

$t\bar{t}$ signal events per dilepton flavor category				
Source	ee	$\mu\mu$	$e\mu$	$\ell\ell$
WW	2.16 ± 0.38	2.42 ± 0.42	4.79 ± 0.80	9.37 ± 1.51
WZ	0.94 ± 0.15	0.68 ± 0.11	0.59 ± 0.10	2.22 ± 0.33
ZZ	0.65 ± 0.51	0.64 ± 0.50	0.23 ± 0.18	1.51 ± 1.18
$W\gamma$	0.23 ± 0.25	0.00 ± 0.00	0.00 ± 0.00	0.23 ± 0.25
DY $\rightarrow \tau\tau$	1.67 ± 0.32	1.76 ± 0.34	3.87 ± 0.72	7.29 ± 1.34
DY $\rightarrow ee + \mu\mu$	11.81 ± 2.16	5.32 ± 1.23	1.36 ± 0.60	18.49 ± 2.73
W + jet fakes	3.91 ± 1.28	9.34 ± 3.05	20.90 ± 6.43	34.15 ± 9.51
Total background	21.37 ± 3.14	20.16 ± 3.64	31.73 ± 6.78	73.26 ± 11.30
$t\bar{t}$ ($\sigma = 6.7$ pb)	28.80 ± 1.41	31.24 ± 1.52	70.15 ± 3.36	130.19 ± 6.21
Total SM expectation	50.17 ± 4.25	51.40 ± 5.00	101.88 ± 10.06	203.45 ± 17.33
Observed	41	55	99	195

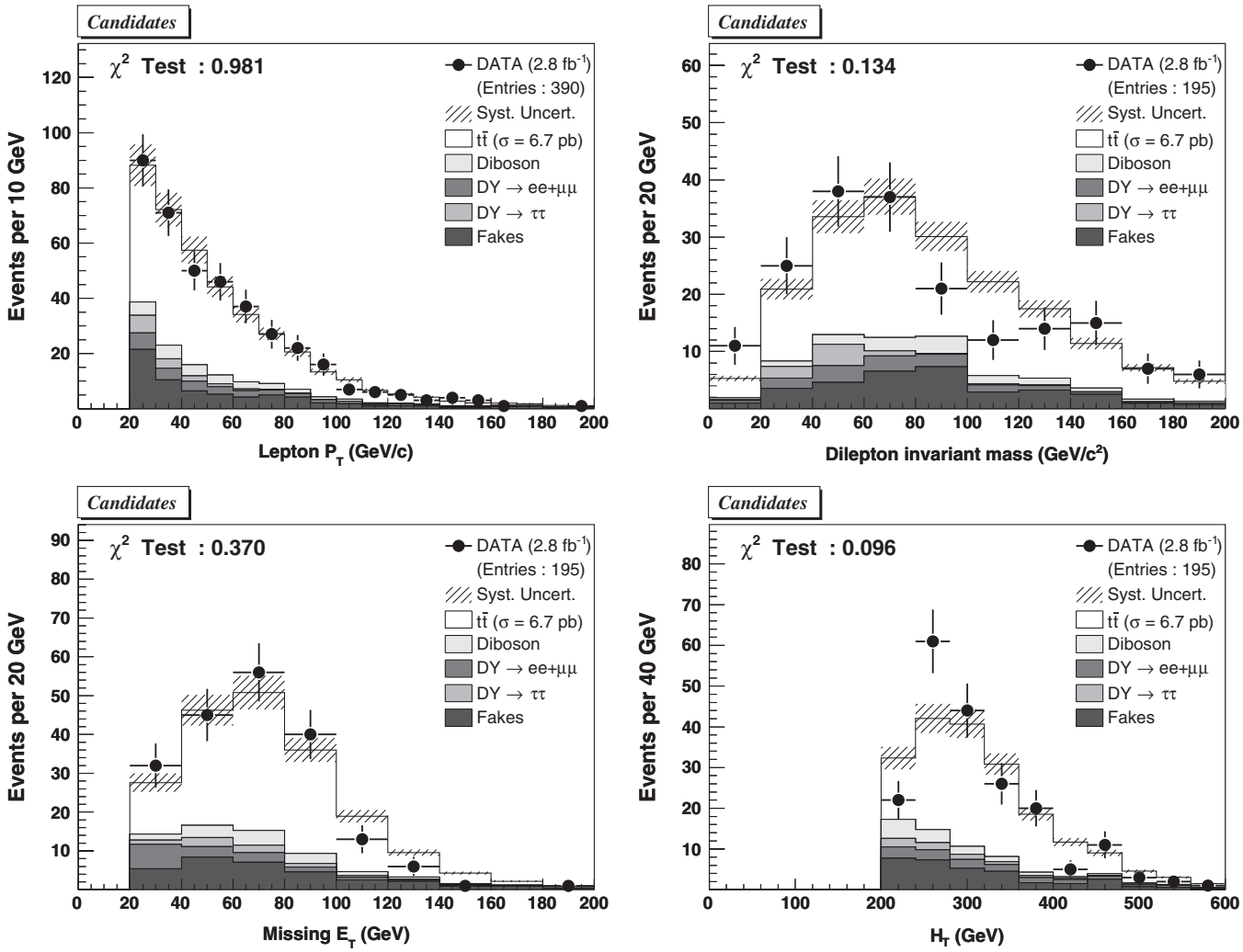

FIG. 8. Background and top quark signal predictions overlaid on the data for top quark DIL candidate events in 2.8 fb^{-1}. From top left to bottom right: Two leptons transverse energy spectrum, the dilepton invariant mass, the event $\not\!\!E_T$ and H_T. The hatched area represents the uncertainty in the total background estimate.

TABLE XIII. Summary table by jet multiplicity bin of background estimates, $t\bar{t}$ predictions, and observed events in data corresponding to an integrated luminosity of 2.8 fb^{-1}. The uncertainties are the sums in quadrature of the statistical and systematic error. The last column contains the candidate events with $H_T > 200$ GeV and opposite sign lepton cuts applied.

Control sample and signal events per jet multiplicity				
Source	0 jet	1 jet	≥ 2 jet	H_T + OS
WW	142.87 ± 12.57	40.01 ± 4.24	14.70 ± 2.47	9.37 ± 1.51
WZ	11.65 ± 0.74	11.72 ± 0.52	4.44 ± 0.57	2.22 ± 0.33
ZZ	8.79 ± 6.78	4.08 ± 3.14	2.04 ± 1.59	1.51 ± 1.18
$W\gamma$	28.03 ± 7.11	8.14 ± 2.27	2.07 ± 0.78	0.23 ± 0.25
DY $\rightarrow \tau\tau$	3.89 ± 0.58	17.87 ± 2.99	12.94 ± 3.22	7.29 ± 1.34
DY $\rightarrow ee + \mu\mu$	40.04 ± 5.77	40.83 ± 7.28	30.13 ± 8.54	18.49 ± 2.73
W + jet fakes	72.49 ± 19.02	94.23 ± 26.16	83.00 ± 22.90	34.15 ± 9.51
Total background	307.76 ± 35.84	216.87 ± 32.46	149.33 ± 28.19	73.26 ± 11.30
$t\bar{t}$ ($\sigma = 6.7$ pb)	0.67 ± 0.06	17.44 ± 0.86	138.56 ± 6.61	130.19 ± 6.21
Total SM expectation	308.43 ± 35.87	234.31 ± 33.28	287.89 ± 34.70	203.45 ± 17.33
Observed	342	219	269	195

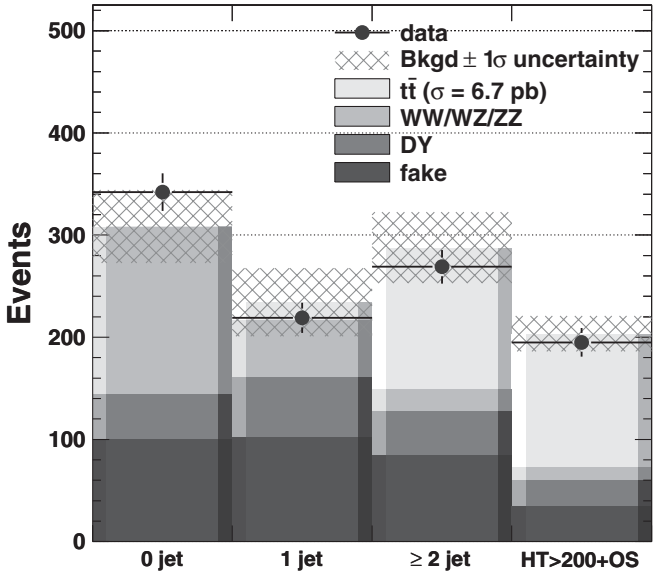

FIG. 9. Dilepton candidate events (black point) by jet multiplicity. The stacked histogram represents the background contribution and the $t\bar{t}$ contribution for an assumed $\sigma_{t\bar{t}} = 6.7$ pb. The hatched area is the uncertainty in the total background estimate.

two or more jets we select a sample with a signal top quark pair almost a factor of 2 larger than the background. The contamination from SM sources is checked in lower jet multiplicity samples. From the excess of data over the background predictions we measure:

$$\sigma_{t\bar{t}} = 6.27 \pm 0.73(\text{stat}) \pm 0.63(\text{syst}) \pm 0.39(\text{lum})\ \text{pb},$$

or

$$\sigma_{t\bar{t}} = 6.27 \pm 1.03(\text{total})\ \text{pb},$$

consistent with the NLO standard model calculation of $6.7^{+0.7}_{-0.9}$ pb. Yields in the ee, $\mu\mu$, and $e\mu$ final states are in agreement with the predictions from lepton universality.

ACKNOWLEDGMENTS

We thank the Fermilab staff and the technical staffs of the participating institutions for their vital contributions. This work was supported by the U.S. Department of Energy and National Science Foundation ; the Italian Istituto Nazionale di Fisica Nucleare; the Ministry of Education, Culture, Sports, Science and Technology of Japan; the Natural Sciences and Engineering Research Council of Canada; the National Science Council of the Republic of China; the Swiss National Science Foundation; the A. P. Sloan Foundation; the Bundesministerium für Bildung und Forschung, Germany; the World Class University Program, the National Research Foundation of Korea; the Science and Technology Facilities Council and the Royal Society, UK; the Institut National de Physique Nucleaire et Physique des Particules/CNRS; the Russian Foundation for Basic Research; the Ministerio de Ciencia e Innovación, and Programa Consolider-Ingenio 2010, Spain; the Slovak R&D Agency; and the Academy of Finland.

[1] D. Acosta *et al.* (CDF Collaboration), Phys. Rev. Lett. **93**, 142001 (2004).
[2] T. Aaltonen *et al.* (CDF Collaboration), Phys. Rev. D **79**, 112007 (2009).
[3] M. Cacciari *et al.*, J. High Energy Phys. 09 (2008) 127; N. Kidonakis and R. Vogt, Phys. Rev. D **78**, 074005 (2008); S. Moch and P. Uwer, Nucl. Phys. B, Proc. Suppl. **183**, 75 (2008).
[4] R. Blair *et al.*, The CDF II Detector Technical Design Report, Fermilab-Pub-96/390-E.
[5] C. S. Hill *et al.*, Nucl. Instrum. Methods Phys. Res., Sect. A **530**, 1 (2004); A. Sill *et al.*, Nucl. Instrum. Methods Phys. Res., Sect. A **447**, 1 (2000); A. Affolder *et al.*, Nucl. Instrum. Methods Phys. Res., Sect. A **453**, 84 (2000).
[6] A. Affolder *et al.*, Nucl. Instrum. Methods Phys. Res., Sect. A **526**, 249 (2004).
[7] L. Balka *et al.*, Nucl. Instrum. Methods Phys. Res., Sect. A **267**, 272 (1988); S. Bertolucci *et al.*, Nucl. Instrum. Methods Phys. Res., Sect. A **267**, 301 (1988); M. Albrow *et al.*, Nucl. Instrum. Methods Phys. Res., Sect. A **480**, 524 (2002).
[8] G. Ascoli *et al.*, Nucl. Instrum. Methods Phys. Res., Sect. A **268**, 33 (1988).
[9] D. Acosta *et al.*, Nucl. Instrum. Methods Phys. Res., Sect. A **494**, 57 (2002).
[10] A. Abulencia *et al.* (CDF Collaboration), J. Phys. G **34**, 2457 (2007).
[11] A. Affolder *et al.* (CDF Collaboration), Phys. Rev. Lett. **88**, 041801 (2002).
[12] F. Abe *et al.* (CDF Collaboration), Phys. Rev. D **45**, 1448 (1992).
[13] A. Bhatti *et al.*, Nucl. Instrum. Methods Phys. Res., Sect. A **566**, 375 (2006).
[14] T. Sjostrand, S. Mrenna, and P. Skands, J. High Energy Phys. 05 (2006) 026. We use version 6.216.
[15] A. D. Martin, W. J. Stirling, R. S. Thorne, and G. Watt (CDF Collaboration), Phys. Lett. B **652**, 292 (2007).
[16] M. L. Mangano *et al.*, J. High Energy Phys. 07 (2003) 001. We use version 2.10. M. L. Mangano, M. Moretti, F. Piccinini, and M. Treccani, J. High Energy Phys. 01 (2007) 013.
[17] J. M. Campbell and R. K. Ellis, Phys. Rev. D **60**, 113006 (1999).
[18] W. Giele *et al.*, arXiv:hep-ph/0204316.
[19] U. Baur and E. L. Berger, Phys. Rev. D **41**, 1476 (1990).

[20] U. Baur, T. Han, and J. Ohnemus, Phys. Rev. D **48**, 5140 (1993).
[21] D. Lange, Nucl. Instrum. Methods Phys. Res., Sect. A **462**, 152 (2001).
[22] T. Aaltonen *et al.* (CDF Collaboration), Phys. Lett. B **692**, 232 (2010).
[23] Tevatron ElectroWeak Working Group for the CDF and D0 Collaborations, arXiv:0903.2503.